Pressure dependence of T_g in silicate glasses from electrical impedance measurements

N. S. Bagdassarov,[1] *J. Maumus*[2]

Institut für Meteorologie und Geophysik, Universität Frankfurt, Feldbergstraße 47, D-60323 Frankfurt/Main, Germany

B. Poe[3]

Bayerisches Geoinstitut, Universität Bayreuth, Universitätsstraße 30, D-95447 Bayreuth, Germany

<u>*A. B. Slutskiy*</u> *& V. K. Bulatov*

Vernadsky Institute of Geochemistry and Analytical Chemistry, Russian Academy of Sciences, Kosyguine str. 19, GSP-1, 117975 Moscow, Russia

The pressure dependence of the glass transition temperature (T_g) has been estimated from the pressure effect on the activation energy of electric conductivity in alkaline (albite, haplogranite), alkaline earth (anorthite) silicate and SiO_2 glasses. The dc conductivity (σ) has been determined from the electrical impedance spectroscopy in the frequency range 10^5–10^{-2} Hz. The impedance measurements have been performed in a controlled atmospheric furnace and in three types of high pressure apparatuses: piston cylinder, belt and multi-anvil presses in the pressure range 0·3–6 GPa. Below T_g, the activation energy of σ is less than that at $T>T_g$. The inflection point on the dependency of $ln(\sigma)$ versus $1/T$ defines T_g. The T_g in anorthite glass varies with pressure as $T_g=848°C+5·3°/GPa\,P$ (P is in GPa), in albite as $T_g=688°C−9·4°/GPa\,P$, in haplogranitic glass as $T_g=777°C−45°/GPa\,P$ and in SiO_2 glass as $T_g =1050°C+50°/GPa\,P$. The measured at T_g dielectric relaxation times are several orders of magnitude smaller than the structural relaxation times and become slower with the increasing pressure. In Na bearing glasses, T_g estimated from the electrical conductivity is a 'sodium ion mobility' T_g^{Na}, corresponding to the temperature range of the overlapped α- and β-relaxation processes and is, therefore, shifted to lower temperatures in comparison with calorimetric and dilatometric T_g. The activation energy of the dielectric relaxation in anorthite increases with pressure having an activation volume of $+10·5\pm5$ cm^3/mol, and in albite glass the activation volume is negative $−6·5\pm2$ cm^3/mol.

---

[1] Corresponding author. Email: nickbagd@geophysik.uni-frankfurt.de
[2] Present address: Université Blaise Pascal, 5 rue Kessler, 63038 Clermont-Ferrand cedex, France
[3] Present address: Dipartomento di Scienza della Terra, Università degli Studi "G. Annunzio" Chieti, Italy
A. B. Slutskiy died on 18 March 2004

Pressure dependence of viscosity and T_g

The glass transition temperature T_g of silicates is the isoviscous temperature at which melts are believed to possess a viscosity $\sim10^{12–13}$ Pa s, and a relaxation time for shear stress of about 100 s.[1] Knowledge of the glass transition temperature at high pressures provides indirect information about the pressure dependent rheology and the effect of glass densification on relaxation processes. This is of special interest in geosciences and in silicate melt physics, where the viscosity measurements at high pressures and temperatures are technically difficult to carry out, while *in situ* rheological measurements require x-ray radiography and synchrotron radiation techniques.[2]

The pressure dependence of silicate melt viscosities at high pressures plays a key role in the prediction of partial melting in mid-oceanic regions and ascent of magma to the earth's surface.[3] For decades, earth scientists have sought a general equation to model the viscosity of magmatic silicate melts as a function of temperature, pressure and composition (see, for example, Refs 4–8). In early viscosity models[4,5] the Arrhenian temperature dependence of viscosity

$$\log\eta_T=A+(\Delta E_a/RT) \tag{1}$$

was suggested, where ΔE_a is the activation energy of viscous flow, A the pre-exponential factor, R the universal gas constant. Equation (1) contains two parameters both of which depend on melt composition. In Ref. 5 the number of fitting parameters in Equation (1) was reduced to ΔE_a (A was assumed equal to $−3·5$ for all substances), making the use of this viscosity model highly impractical. Recent experimental results demonstrate that Equation (1) is not adequate for most silicate melts over a wide temperature range.[6,7] In recent years some new models of viscosity have been applied to sili-

cate melts by the use of VFT (Vogel–Fulcher–Tammann) equation instead of the Arrhenius type[7,8]

$$\log\eta_T = A + (B/T - T_o) \tag{2}$$

or on the basis of the WLF (Williams–Landel–Ferry) equation, where the three constants A, B and T_o in Equation (2) are replaced to $A = \log\eta_{T_g}$, $B = B^*(T_g - T)$ and $T_o = (T_g - T^*)$, respectively.[6] In Equations (1,2), η_T is the viscosity at temperature T, and A, B, T_o are the empirical constants. In a modified form of Equation (2), $\log\eta_{T_g}$ is the viscosity at the glass transition temperature T_g. In contrast to the temperature dependence, the pressure dependence of magmatic melt viscosity is poorly described. There have been a few attempts to generalise the viscosity dependence on pressure: (1) either by introducing a pressure dependent activation energy in Equation (1)[5] or (2) by applying a modified form of Equation (2), a WLF type equation, and correcting the glass transition temperature $T_g(P)$ for pressure.[6] One unclear point in the latter approach concerns the type of glass transition temperature to be used in T_g dependent constants B and T_o: rheological, calorimetric, dilatometric, etc?

A second unclear point in a WLF type of equation is the dependence of T_g on cooling rate q, which has to be taken into account; T_g is measured by different probing methods. What method of T_g estimation is better, cooling–heating temperature scans in a time domain or dynamic measurements in a frequency domain? The general dependence of T_g as a function of cooling rate q, is as follows

$$\frac{d \ln|q|}{dT_g} = \frac{\Delta E}{RT_{T_g}^2} \tag{3}$$

where ΔE is the activation energy of the physical property used for detecting T_g.[9,10] Thus, for samples with differing thermal histories, one may expect differing unrelaxed states of the supercooled melt at T_g and the uncertainty in viscosity estimations by applying the T_g dependent constants in Equation (2) may be large. In any case, the step in relating viscosity and pressure may be the experimental or theoretical estimations of a glass transition temperature as a function of pressure for samples having the same q.

A general way to describe the pressure dependence of $T_g(P)$ is to modify Equation (3) by correcting ΔE at normal pressure (superscript index 1) for some pressure–volume effect

$$T_g(P) = T_g^1 \left[1 + \frac{P\Delta V}{\Delta E^1} \right] \tag{4}$$

or

$$\frac{dT_g}{dP} = T_g^1 \frac{\Delta V}{\Delta E^1} \tag{5}$$

where ΔV is the activation volume of the physical property used to determine T_g and index 1 refers to the property at normal pressure.[11]

A different approach was suggested by considering the glass transition as a second-order phase transition. In this case, a Clayperon slope of T_g with pressure must obey

$$\frac{dT_g}{dP} = \frac{\Delta\beta_T}{\Delta\alpha_p} \tag{6}$$

and

$$\frac{dT_g}{dP} = \frac{TV\Delta\alpha_p}{\Delta C_p} \tag{7}$$

where $\Delta\beta_T$ is the change of the isothermal compressibilities, and $\Delta\alpha_p$ is the change of isobaric expansivities, and ΔC_p is the difference in the isobaric heat capacity between liquid and glass.[12–15] Combination of Equations (6) and (7) (two Ehrenfest equations) provides a so-called Prigogine–Defay (PD) ratio, Π

$$\Pi = \frac{\Delta C_p \Delta\beta_T}{T_g V \Delta\alpha_P^2} = 1 \tag{8}$$

A number of experiments have been done on polymers, low temperature glass formers and silicates to test the validity of Equations (6)–(8).[12, 16–19] Usually, the value of the PD-ratio, Π, is much greater than 1 ($\Pi\sim$ varies from 2 to5). This violation has been attributed to to the nonequilibrium nature of the glass transition[20] where one 'ordering parameter' does not adequately describe a phase transformation. In some works, this problem was solved by introducing an additional 'ordering parameter' to generalise the Ehrenfest equations for the case of the glass transition (e.g. Refs 20, 21).

In many studies of the glass transition, it has been demonstrated that the first Ehrenfest equation, Equation (6), may be satisfied automatically by a proper calculation procedure of the volume derivatives in respect to pressure and temperature.[13,14] In the derivation of the second Eherenfest equation the free Gibbs energy ΔG must be corrected to the effect of the configurational entropy $-T_e x \Delta S_{conf}$, where $T_e > T$ an effective temperature at which processes related to the configurational entropy are 'thermalised'.[14] In this way, the correctly calculated PD ratio may be very close to 1 for some glass formers.

As an alternative to the thermodynamic approach mentioned above, there has been an attempt to describe the pressure dependence of the glass transition by use of the VFT relation, Equation (2), replacing the temperature T by a pressure variable P. If τ is the shear stress relaxation time, which relates to the relaxed shear viscosity as $\tau \sim \eta/G$ (G is unrelaxed shear modulus), then

$$\tau = \tau_o \exp(B/(P_o - P)) \text{ at } T = \text{const} \tag{9}$$

derived from a free volume model (e.g. Ref. 22). By analogy with temperature glass transition, the pressure glass transition is characterised by a pressure P_g, at which the relaxation time is 10^2 s and P_o is an ideal glass transition pressure at which the viscosity exponentially diverges, (by analogy with T_o in Equation (2)), τ_o denotes the relaxation time at normal pres-

sure 0·1 MPa. In some isothermal experiments, this behaviour of the viscosity was observed.[23,24]

On the basis of the isothermal dielectric relaxation time measurements on supercooled strong liquids, another expression was suggested, where the parameter B in Equation (9) is $\propto P$.[22] The general expression of the relaxation time (or viscosity) can be considered in this case to be of the form of Equation (2), where B and T_o are linear functions of pressure.[25,26] Equation (2) or VFT equation in this extended form has been tested on specific heat spectroscopic measurements (enthalpy relaxation) with unsatisfactory results for fragile glass formers.[25]

The failure of the universal pressure–temperature superposition principle is explained by the fact that the glass transition is considered as a simple volume activated process ($\ln \tau \sim 1/V_f$ and V_f is free volume). The free volume in this approach is believed to depend on pressure and temperature in the same way through a constant compressibility and thermal expansion coefficient. This is not true for many classes of glass forming materials such organic glass formers, the free volume V_f is not a linear function of pressure. Contrary results were obtained for the dielectric relaxation of epoxy resin, where relaxation times are suitably described by the extended VFT equation, i.e. Equation (2) with the linear dependence of the constants B and T_o on pressure.[22] To construct an expression for viscosity of magmatic silicate melts according to an extended form of Equation (2), taking into account a linear dependence of B and T_o on pressure, would require five fitting parameters (two constants for the linear pressure dependence of B, two constants for pressure dependence T_o and a constant A) obtained from a large number of relaxation experiments at different pressures and temperatures. According to a modified Equation (2) in a form of the WLF equation, we need only three fitting parameters and independent data on $T_g(P)$.

Another important glass parameter needed for characterisation of glass formers is the fragility index m, which represents the extent of the liquid's deviation from Arrhenian behaviour and can be defined as follows

$$m = \left[\frac{1}{2\cdot303}\frac{\mathrm{d}\ln\tau}{\mathrm{d}\left(T_g/T\right)}\right]_{T=T_g} = \left[\frac{\mathrm{d}\log\left(\eta\right)}{\mathrm{d}\left(T_g/T\right)}\right]_{T=T_g} \quad (10)$$

(e.g. Ref. 27). From Equations (2) and (10) it follows that the fragility index m depends on T_g as

$$m = \frac{1}{2\cdot303}\frac{T_g B}{\left(T_g - T_o\right)^2} \quad (11)$$

where $T_o < T_g$. If a modified form of Equation (2), a WLF equation, is used for the viscosity model, then

$$m = \frac{1}{2\cdot303}\frac{B^* T_g}{T^*} \quad (12)$$

The dependence of m on pressure is unknown. According to Equation (11) the positive dependence of

T_g on pressure will result in decreasing m (denominator is a stronger function of T_g than numinator) and, therefore, a liquid under pressure becomes stronger, which was observed in dielectric relaxation experiments with epoxy resin.[22] If $\mathrm{d}T_g/\mathrm{d}P$ is negative, then m increases with pressure and a liquid is more fragile. Contrary to conclusions obtained by using Equation (12), the viscosity model described by a modified Equation (2), predicts an increase or decrease of the fragility index m directly proportional to the pressure dependence of T_g. This simply means that the modified Equation (2) (WLF equation) and Equation (12) may only be applicable if the fragility parameter m is small, i.e. for very strong liquids ($T_g \gg T_o$) in which the divergence temperature T_o is far away from T_g.

The relaxation model of Avramov,[28] based on the entropy description of the glass transition, predicts viscosity and structural relaxations as a function of pressure and temperature. According to the configurational entropy theory of Adam and Gibbs, transport processes in the liquid state occurs *via* rearrangements of structural clusters or subunits. The entropy of these units to rearrange is a minimum configurational entropy. The rearrangement probability of structural subunits is an exponentially decaying function of the free energy barrier to rearrangement divided by a minimum configurational entropy of the cooperatively rearranging cluster $S_{conf}(T)$ and absolute temperature T. Both of them, free energy barrier and configurational entropy, can be, in principle, pressure dependent. The model of Ref. 28 assumes a Poisson distribution of the Adams–Gibbs energy barriers of jump frequencies at T_g with a dispersity factor exponentially proportional to the excess of the configurational entropy relative to a reference state.[28] The temperature and pressure dependence of the relaxation time τ in the frame of this phenomenological theory is as follows

$$\tau = \tau_0 \exp\left\{\varepsilon\left(\frac{T_g}{T}\right)^{a}\left(1+\frac{P}{P*}\right)^{b}\right\} \quad (13)$$

where $\varepsilon = \Delta E/RT_g$ is the dimensionless activation energy at T_g ($\sim 30\cdot5$ for silicate glasses), a plays a role of a fragile parameter, b is the dimensionless constant which depends on the coordination number Z of the liquid lattice, $P*$ is the pressure constant estimated from an empirical relationship of the thermal expansion coefficient κ upon pressure $\kappa = \kappa_0(1+(P/P*)^{-1}$.[29] By introducing a pressure dependence of the coordination number Z, Equation (13) demonstrates a good agreement with experimental results on some polymer glass formers. After a substitution of Equation (13) in Equation (10) and neglecting the pressure dependence of constants a, b and C_p, the fragility index m depends on pressure as follows

$$m = \frac{\varepsilon\left(1+\left(P/P*\right)\right)^{b}}{2\cdot303}\left(a - \frac{bT_g}{\left(P+P*\right)}\left[\frac{\mathrm{d}P}{\mathrm{d}T}\right]_{T=T_g}\right) \quad (14)$$

Thus, depending on the sign of pressure dependence of T_g, the fragility index m may increase or de-

crease with pressure. In other words, the densification of glass under pressure and fragility index m are correlated via Equation (14). In fact, such a correlation simply reflects the sensitivity of T_o/T_g variation in respect to pressure P.

The main purpose of this paper is to examine the pressure dependence of T_g obtained from dielectric spectroscopy measurements at high pressures on silicate glasses having differing fragility indices m, and the coupling between viscous and dielectric relaxations. In this work, estimates of T_g in some silicate glasses have done by the use of bulk (dc) electric conductivities measured under pressure.

Estimation of T$_g$ *from electrical impedance spectroscopy*

The electrical conductivity was used as a probing tool to detect T_g at high pressures. To estimate a glass transition temperature at high pressure, we have used a method of defining the activation energy of bulk electrical impedance (or conductivity) in the glass transition temperature range. Despite a 'decoupling' of the macroscopic viscosity and its relaxation time from electrical conductivity relaxation, the kink in a slope of the dc electrical conductivity plotted as function of $1/T$ can be used as an indicator of T_g.[30,31] For glasses with weakly coupled viscous and dielectric relaxation, the Arrhenius dependence of the ac conductivity (measurements of the electrical conductivity at a constant frequency), shows two inflection points, below and at T_g.[30] The inflection point below T_g is frequency dependent and is due to a frequency effect when the experimental time approaching the Na hopping time. It can be seen only for ac conductivity curves and mostly for glasses with the weakly coupled viscous and dielectric relaxations, for example a sodium trisilicate.[30,32] In fact, when dc conductivity data is used, the Arrhenius plot has only one inflection point corresponding to T_g.[30]

For strongly coupled glasses, like SiO$_2$ and anorthite, the first inflection point seen during heating is at T_g, the 'instrumental' inflection points on ac conductivity curves are at $T > T_g$ above glass transition. In Ref. 32 the author argued that the inflection point of electrical conductivity and Na tracer diffusion data at T_g result from the duration of experiments approaching the structural relaxation time. According to Ref. 33, the electric transport processes in alkaline or weakly coupled glasses consist of (1) a local charge separation or dipole electric formation/reorientation (i.e. local displacement of Na$^+$ in polar units near a nonbridging oxygen), (2) a translation motion of Na between adjacent polar units and (3) a long range translational motion of Na between structural positions like a Frenkel point defect. The first two processes occur around the same or neighbour oxygens with a low activation energy giving a rise to dielectric losses and polarisation and not correlating with a diffusion process of alkalis. The third process occurs in a length scale between two nonbridging oxygen/sodium sites and correlates with an alkaline tracer diffusion in the case, when these sites are the nearest and the cooperativity of the charge transport is absent.[34] In strongly coupled glasses (SiO$_2$,

anorthite) where alkalis are at the dilute limit, the contribution to the electric conductivity is only from the latter process. In the case of albite or in other aluminosilicate glasses where there are no nonbridging oxygens, the polar units are formed by a sodium ion and an oxygen atom participating in AlO$_4^-$ units.

The interpretation of the inflection points on dc conductivity curves at $T \sim T_g$ is given in Refs 30, 35. Electrical conductivity is always associated with a mobility of 'loose' particles (alkaline atoms or impurities) whose ability to self diffusion or polarisation is higher than other species in the structure. The essential thing for this mobility decoupling is that these 'loose' particles always represent a small subset of the structure, i.e. the transport of this particles does not influence the structural relaxation (α-relaxation) at $T < T_g$. Thus, below T_g, the slope of conductivity is determined by a free energy barrier for Na$^+$ and not for the oxygen or Si atoms, in case of sodium silicates. At $T > T_g$ the matrix itself starts to relax, the mean squared displacements of oxygen atoms $<r^2>$ become significant and this results in an increase of the energy barrier for Na$^+$ transport (conductivity or diffusion). Such a change is detected as an increase of slope of dc electrical conductivity in an Arrhenian plot at $T \sim T_g$.[30,31,35] The detected T_g is a 'cation glass temperature';[35] it depends on the relative abundance of nonbridging oxygens, alkalis and Q$_n$ species.[34] Many recent papers on the structure of *Na* silicates and Na aluminosilicates with varying ratio of Al$_2$O$_3$/Na$_2$O,[34,36] demonstrate a nonhomogeneous distribution of alkalis nonbridging oxygen pairs (channelling) and a clustering of AlO$_4$ groups in three dimensional structures. The inflection point at T_g on conductivity and diffusion curves, in these microsegregated structures, can be understood as a starting temperature for the smoothing out of channel and cluster boundaries. The transport of alkalis below T_g is believed to occur predominantly along those pathways where alkalis, nonbridging oxygens and/or AlO$_4$ groups are microsegregated; this serves as a physical background for a non-Fickian diffusion and a compositional dependence of a Haven coefficient accounting for a cross correlation effect of diffusion at the nondilute limit of the diffusing species.[37]

Experiments

Description of samples

The impedance measurements were performed on glass samples of anorthite (CaAl$_2$Si$_2$O$_8$), albite (NaAlSi$_3$O$_8$), haplogranitic (HPG8) composition glass and SiO$_2$. Compositions of silicate glass samples that were used in impedance spectroscopy experiments are listed in Table 1. In the present study we have compared the pressure dependence of T_g for four different glasses. Their fragility index m calculated according to Equation (10) is shown in Figure 1. Besides the differing fragility index m and plots of viscosity vs T_g/T in the spirit of the Angell classification (e. g. Reference 38), these glasses have very different structures and mechanisms of the electrical conductivity. They can be classified as 'loose' (albite and haplo-granitic glasses), 'tight' and 'fragile' (anorthite), and 'tight' and 'strong'"
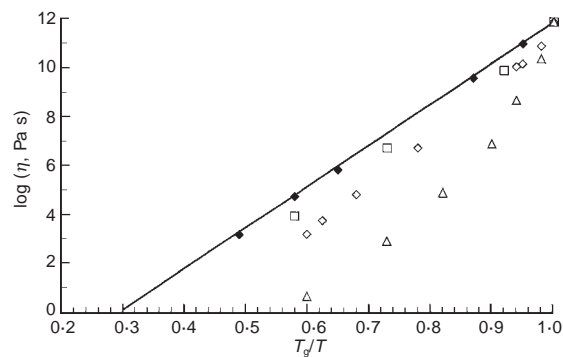
Figure 1. *Angell plot of samples used in the electrical conductivity study. The fragility index varies from 17 for SiO$_2$ to 42 for anorthite.* [38] *Viscosity data for haplogranitic glass HPG8 are from Ref. 39*
—— strong liquid   ◆ SiO$_2$ m=17   □ Albite m=19
◇ HPG8 m=21·5[39]   △ Anorthite m=42

(SiO$_2$) conducting glasses,[35] accordingly.

The samples of anorthite and albite glass were taken from the glass collection of M. Rosenhauer (Göttingen), HPG8 was provided by D. Dingwell (München), and SiO$_2$ glass is a commercial glass Suprasil 300 (Heraeus, Germany), containing <1 ppm of OH$^-$. The haplogranitic glass (HPG8) corresponds to the eutectic composition of SiO$_2$.NaAlSi$_3$O$_8$.KAlSi$_3$O$_8$ at 0·1 GPa P$_{H_2O}$. The interest in HPG8 glass in the present study is also due to the fact that many physical properties of this glass have been measured in recent years.[40]

Impedance spectroscopy measurements

Electrical impedance measurements were carried out using a Solartron 1260 phase-gain-analyser interfaced with a PC. The device permits a single sine drive and analysis of a system under test over the frequency range 10μ Hz to 32 MHz. In the high pressure experiments we applied a 1 V sinusoidal signal over the frequency range from 0·01 Hz to 100 kHz. Typically, the frequency scan utilised logarithmic steps of 0·2–0·5. Signals at higher frequencies were affected by cable impedance and at lower frequency signals became too noisy. The estimation of the 'bulk' electrical conductivity from frequency scans provide 'true' dc conductivity data and, therefore, the artefact due to a mismatch of the probe frequency and material relaxation times can be avoided.[30,35]

Measurements at 0·1 MPa

For measurements in the atmospheric furnace, Figure 2, glass samples (diameter *D*=6 mm, 8 mm for silica
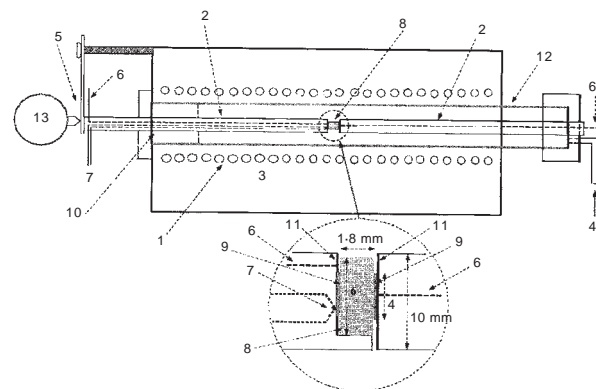

Figure 2. *Scheme of the electrical conductivity experiments at 0·1 MPa: 1 Pt-wire furnace ROR Heraeus; 2 Al$_2$O$_3$ ceramic rods AL23 Frialit-Degussit; 3 insulating casting body; 4 inlet for inert gas (Ar); 5 flat spring; 6 electrode contact of Pt-wire; 7 thermocouple S-type Pt-PtRh; 8 sample of glass; 9 sputtered area of sample; 10 tephlon guiding plug; 11 Pt-folio cemented to the surface of Al$_2$O$_3$ rods; 12 inner Al$_2$O$_3$ tube; 13 elongation gauge*

glass) were drilled out of blocks of glass and cut into discs with thickness *L*=1–1·5 mm. Flat surfaces were polished with 0·05μ alumina powder to optical quality of the surface. The sample of silica glass was polished down to 0·5 mm thickness. Pt electrodes (thickness= 5μ) were sputtered onto both flat surfaces of the glass discs (spot diameter 4·85 mm). On the silica sample, the electrodes were sputtered with a spot of 8 mm in diameter. The samples were mounted in the inductive furnace (Heraeus, Hanau, Germany) with the heating element made of Pt wire. During the measurements, samples were fixed between alumina rods (Frialit-Degussit with flat electrodes made from Pt foil. The elongation of the sample was measured with a micrometer gauge having a precision of 0·001 mm. Electrical contact between Pt foil and sputtered electrodes was provided by a light flat spring acting axially through one of the alumina rods. The heating rate of the furnace was approximately 20°/h. A type S thermocouple (Pt–PtRh$_{10}$) touched the Pt foil which was in direct contact with the sample. Electrical impedance measurements were done only once on each sample during the heating cycle. The geometric factor of samples *G*=π*D*²/4*L*, for albite, anorthite and HPG8 ranged from 1 to 1·3 cm, and for silica glass was approximately 10 cm. Temperature was measured and controlled using a Eurotherm 818P.

Measurements in piston cylinder apparatus

For the moderate pressure experiments (0·3–1 GPa), a conventional piston cylinder apparatus with an end load was used. The measurements of the electrical impedance were performed at pressures up to 1 GPa and temperatures up to 1200°C (see Ref. 41 for details). The inner part of a high pressure cell is shown in Figure 3. The pressure calibration of the cell was determined using some standard point materials: at room temperature the transformations Bi I–II–III at 2·56 and 2·7 GPa were used; at high temperature, melting curves of NaCl and CsCl and the α–β transition in LiNaSO$_4$ were used as standard points.[41]
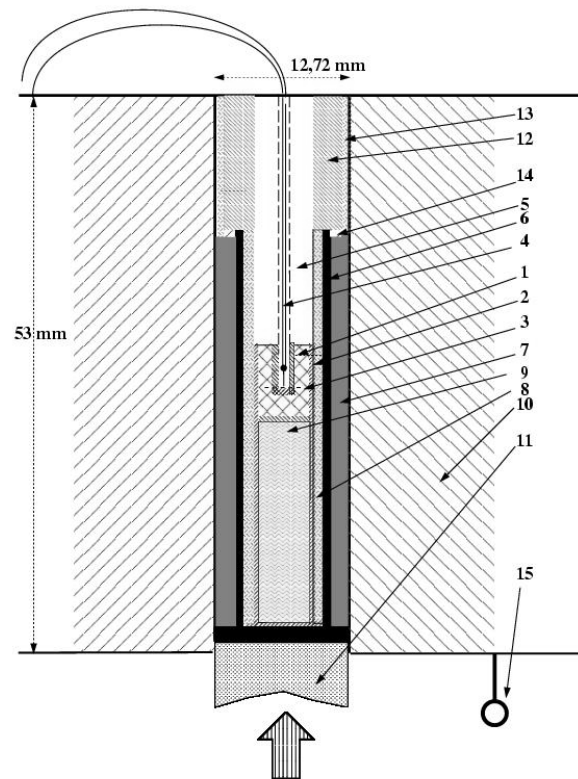
Table 1. *Composition of glass samples (wt%)*

Oxide	CaAl$_2$Si$_2$O$_8$		NaAlSi$_3$O$_8$		HPG8
	Starting composition	After experiment	Starting composition	After experiment	
SiO$_2$	42·63	42·62	67·76	67·53	77·9
Al$_2$O$_3$	36·86	37·14	19·58	21·37	11·89
Na$_2$O			12·09	10·39	4·53
K$_2$O			0·21	0·27	4·17
CaO	20·13	19·89	0·18	0·21	
Sum:	99·62	99·65	99·82	99·77	98·48
Cooling rate, K/h	20		0		300

Microprobe analysis JEOL JXA – 8900RL, 20 kV, sample current 20nA, average of 3–5 points

Figure 3. *Principal scheme of a piston-cylinder cell used for electrical impedance measurements:*[41] *1 inner cylindrical Pt-electrode; 2 outer cylindrical Pt-electrode; 3 sample; 4 thermocouple S-type; 5 Al$_2$O$_3$ ceramic; 6 graphite heater; 7 CaF$_2$ pressure transmitting medium; 8 bornitride; 9 boron nitride ceramic; 10 hard metal core; 11 hard metal piston; 12 plug of stainless steel; 13 unfired pyrophyllite; 14 copper-ring; 15 ground*

A cell for electrical impedance measurements in the piston cylinder utilised a coaxial cylindrical capacitor with a geometric factor of 7–8 cm. The exact geometric factor G of the cell was evaluated independently from calibration measurements on NaCl solutions (0·01–3 м) at 22°C and atmospheric pressure. The measured conductivity of NaCl solutions was compared with table values. The calculated geometric factor of a cylindrical capacitor

$$G = 2\pi \frac{L}{\ln(D/d)} \qquad (15)$$

was corrected according to the measured geometric factor in calibration experiments for 25%. In Equation (15) D is the diameter of an outer electrode, d the diameter of an inner electrode and L the length of the cylinder. Measurements of the geometric factor of the cell after high pressure experiments revealed that due to the cell deformation under pressure L increases by ~3–4%, D increases by 1–2% and d remains constant. Overall, these variations of the cell dimensions did not affect the results of T_g or dielectric relaxation measurements.

Experiments in belt apparatus and multianvil press

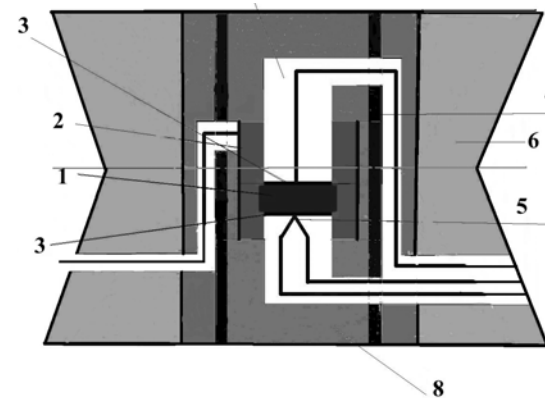A detailed description of the belt apparatus can be found elsewhere.[42] The construction of the experi-

Figure 4. *Principal scheme of the electrical impedance measurement in belt apparatus (height 16 mm*[42]*): 1 sample (diameter 2·1 mm, thickness 1 mm); 2 electrical shield from Pt-foil; 3 electrodes from Pt-foil ; 4 Al$_2$O$_3$ ceramics; 5 thermocouple S-type; 6 pyrophyllite; 7 graphite heater; 8 boron nitride*

mental cells for belt (Figure 4) and multi-anvil apparatus (Figure 5) has the same principle used in Ref. 43. The geometry of the cell was a parallel plate capacitor with a geometric factor approximately 0·3 cm. Metallic electrodes were made from Mo foil. The cell is protected from electrical noise of the graphite (belt apparatus) or LaCrO$_3$ (multi-anvil press) heater by a grounded shield of Mo foil. During the electrical impedance measurements in both apparatus the automatic temperature control was switched off. The temperature was regulated manually through a power thyristor.
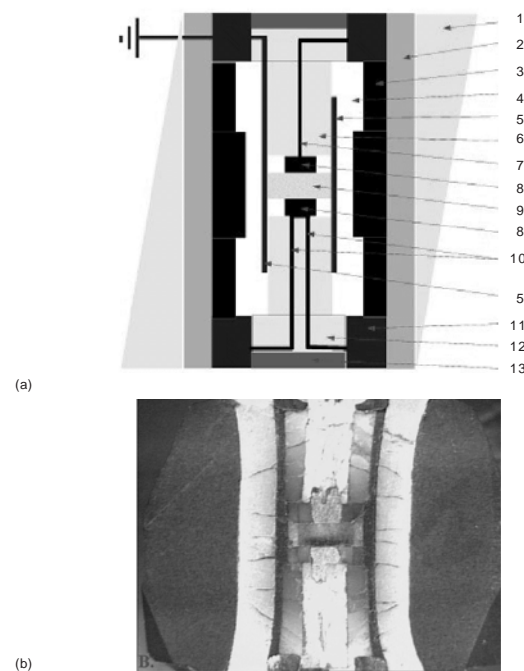

Figure 5. *(a) Principal scheme of electrical conductivity measurements in multi-anvil press:*[43] *1 MgO; 2 ZrO$_2$; 3 LaCrO$_3$ furnace; 4 MgO; 5 Mo shield; 6 Al$_2$O$_3$; 7 electrode wire; 8 Pt electrode; 9 sample; 10 thermocouple wire (electrode); 11 Mo; 12 Al$_2$O$_3$ cement; 13 pyrophyllite. (b) Cross section of the cell with anorthite glass sample after experiment. Thickness of the sample is 1 mm, diameter 2·1 mm*
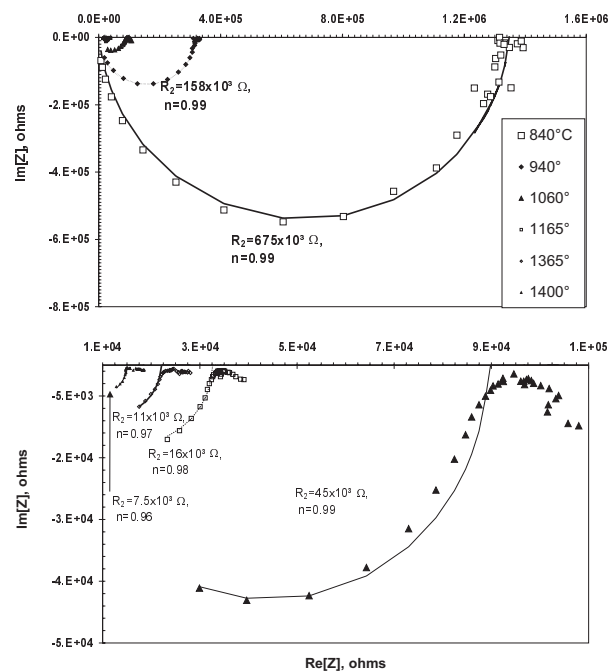
Figure 6. *Argand diagram of Suprasil 300 silica glass at 0·5 GPa. The bulk resistance* R_2 *is estimated from fitting of the impedance scans to Equation (16).* R_2 *also corresponds to the intersection* Im(Z)-*plot with the* Re(Z)-*axes. The impedance arc represents a perfect semicircle. With temperature increase the deviation from Debye relaxation slightly increases, i.e. parameter* n *decreases. Thus, silica glass belongs to a class of 'tight' and strong glassy conductors*[35]

DC electric conductivity from impedance scans

For each sample the electrical conductivity was measured only during a single heating cycle. In both configurations, one of the thermocouple wires was connected to one electrode of the cell with the ac bridge. During the frequency scan the temperature indicator was disconnected from the thermocouple in order to avoid coupling of the two devices at low frequencies.

For each glass sample, the impedance has been measured over the frequency range f from 0·01 to 10^5 Hz. A bulk electrical conductivity of glasses has been estimated from Argand plots generated from these measurements or by fitting a procedure for impedance spectra discussed below. The complex resistance Z measured as a function of angular frequency $\omega = 2\pi f$, can be fitted to a sum of two relaxation functions

$$Z = \frac{R_1}{1 + \left(j\omega\tau_{e.p.}\right)^p} + \frac{R_2}{1 + \left(j\omega\tau_{d.l.}\right)^n} \qquad (16)$$

where the first term in the right hand side of Equation (16) (R_1, $\tau_{e.p.}$ and p) corresponds to the electrode polarisation process and the second term (R_2, $\tau_{d.l.}$ and n) stands for the bulk dielectric losses in the sample.[44] The fitting of data to Equation (16) has been done using Argand plots. The Argand diagram is a complex plane locus in which the imaginary part of the complex impedance $Im[Z]$ is plotted against the real part $Re[Z]$ and each point is characteristic of one frequency measurement. Figure 6 illustrates the Argand plots measured for SiO_2 at 0·5 GPa. The intersection of the

arc with the $Re(Z)$ axes defines R_2, the bulk resistance of the sample. From R_2 and the geometric factor G from Equation (15), the bulk electric conductivity has been calculated, $\sigma_{dc} = 1/(R_2 \times G)$. In the case of SiO_2 and anorthite, we compared the dc electric conductivity with results measured at a constant frequency 10^3 Hz. The electrical measurements of the bulk resistance were measured covering a temperature range below and above T_g. The Arrhenius plots of $\ln(\sigma_{dc})$ versus $1/T$ indicate a change in slope of the conductivity curve at temperature $T \sim T_g$. Measurements of dc conductivity from Argand plots and isofrequency measurements provide about the same T_g for albite and haplogranite glasses but result in significantly differing T_g values for anorthite and silica glasses.

When the fitting of frequency scans of the electric impedance does not permit a reliable estimation of R_2 from fitting Equation (16), the dc conductivity σ_{dc} has been estimated from Argand plots as an intersection of $-Im(Z)$ graph with $Re(Z)$ axes.[44] On an Arrhenius diagram the σ_{dc} data show two distinct slopes with differing activation energies

$$\sigma_{dc} = \sigma_{0,dc} \exp\left(-\frac{\Delta E_a}{RT}\right) \qquad (17)$$

The kink point on plots $\ln(\sigma_{dc})$ versus $1/T$ was used as a characteristic temperature point to discriminate glassy and liquid states only during the first heating cycle (e.g. Refs 30, 31, 45, 46).

Results

Results of 0·1 MPa experiments

The results of electrical conductivity measurements at 0·1 MPa on albite, haplogranitic, anorthite and silica glasses are presented in Figure 7. Electrical conductivities of Na bearing glasses (haplogranite, albite) are 10^4 to 10^5 times higher than those of anorthite and SiO_2 glasses at comparable temperatures. This difference is attributed to the easy dipole polarisation of sodium bearing glasses. High conductivity in these glasses associated with mobility of Na^+ ions which diffusivity is higher than other species. Above T_g the rotation and translation movement of Na cations around nonbridging oxygen atoms contribute to the electrical conductivity of Na^+ bearing glasses at high frequencies (>10^2 Hz). The observed kink of the slope in an Arrhenius plot $\ln|Z|$ versus $1/T$ (where Z is the bulk impedance and T the absolute temperature) or conductivity $\ln\sigma_{dc}$ versus $1/T$, measured at high pressure for Na bearing glasses is significantly lower (>50°C) than T_g estimated from calorimetric and rheological measurements at 0·1 MPa.[46,50] For anorthite and silica glasses the observed kink in the slope is slightly lower than the calorimetric T_g.[51]

As mentioned above, for glasses with alkalis, like Na^+ in albite and haplogranitic glass, the activation energy of σ_{dc} depends on the mobility of Na^+ in the structure. On cooling, at a certain temperature the mobility of a translation motion of alkali ions is not correlated with the thermal structural modifications.[35] In the melt phase, structural elements may always be ar-
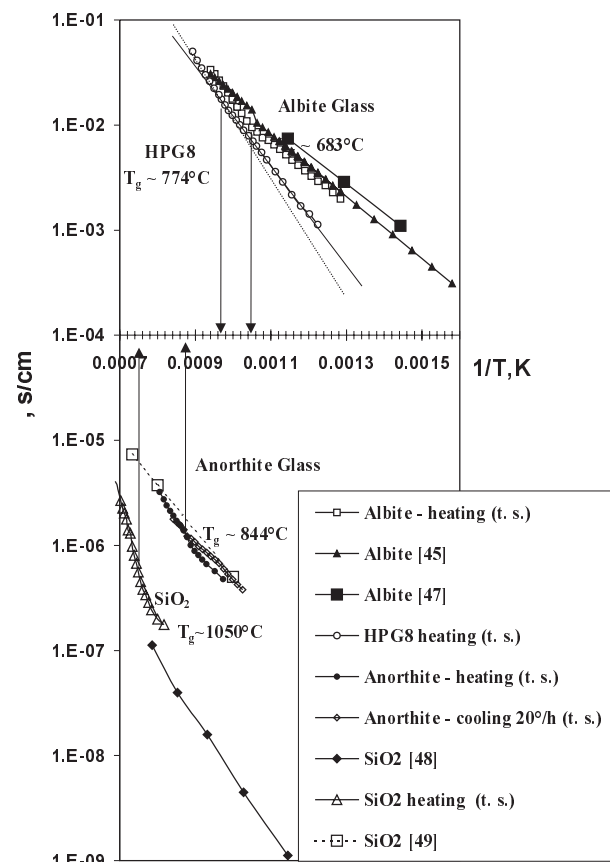
Figure 7. *Results of the bulk electrical resistance σ_{dc} measurements at 0·1 MPa. The kink in the slope of the Arrhenius dependence of the bulk electrical conductivity indicated by arrows. The glass transition temperature T_g is a 'mobile charge carriers (cations) T_g' in the structure of Ab, HPG and An glasses. In SiO_2 glass the charge carriers are impurities, like OH-species and alkalis at a dilute limit*

ranged in an energetically favourable network, leaving minimum space for mobile charged species like Na^+. The experiments confirm that Na bearing silicates the activation energy of σ_{dc} above the glass transition temperature is higher than below T_g. Below the glass transition the mobility of Na^+ remains rather high and is decoupled from the structural relaxation of SiO_4–AlO_4

matrix (α relaxation). This is a reason for the high frequency relaxation processes in Na bearing silicates which has the features of β relaxation. The inflection point on the Arrhenius plot of dc conductivity versus $1/T$ is shifted toward lower temperatures relative to the structural T_g of SiO_4–AlO_4 matrix because of the interaction of two relaxation processes, α and β relaxations. Thus, for alkali bearing systems the temperature at which the kink point is observed in electrical conductivity measurements is different from the glass transition temperature estimated from rheological, heat capacity, or dilatometric experiments, see Table 2. In previous estimations of E_a from electrical measurements above and below T_g the reported ΔE_a values are significantly different: for albite ΔE_a is ~57 and ~60 kJ/mol below and above T_g, respectively;[45] for anorthite at 10 kHz, ΔE_a is 118 and 9·3 kJ/mol.[46] For silica glass containing OH impurities the reported value of ΔE_a for σ_{dc} at $T<T_g$ is ~97 kJ/mol.[48] Measurements on silica glass films $T \ll T_g$ at 20–300°C in which alkalis and OH groups presented at a dilute limit, indicate much smaller activation energy for σ_{dc} ~39 kJ/mol[61] which was identified as the hole like polaron hopping energy.

Structure of glasses and electrical conductivity at 0·1 MPa

The significant difference in electrical conductivity of silica and feldspar glasses might be understood from their differing structures. The structure of feldspar and silica glasses has been determined by x-ray radial distribution analysis.[62] Silica glass has a trydimite like bonding topology based on stuffed six membered rings of SiO_4 tetrahedra. Albite glass has the same structure as silica with aluminium substituting for silicon in some of the tetrahedral sites. In order to accommodate sodium cations such a structure has more 'void spaces and interstices' between rings than SiO_2.[62] In anorthite, the glass structure is based on four membered rings of SiO_4 and AlO_4 tetrahedra.

The mechanism of electrical conductivity in feldspar and silica glasses may be described as a hopping of alkali ion (Na^+ in albite; Na^+ and K^+ in HPG8) or Ca^{2+} (in anorthite) from one near Al oxygen site to another.

Table 2. *Glass transition temperature T_g (°C) at 0·1 MPa*

Glass	Cooling rate (K/h)	Viscosity	Calorimetry and DTA	Volume expansion	Electrical conductivity	Light scattering
SiO_2	slow(?)	1150±20[54]	1180±70[52]	1100±20[53]	1050±10(t.s.)	1100±20[18]
	slow(?)		1190±25[55]			
	100					1050±10[56]
$CaAl_2Si_2O_6$	5	839[38]	865±3[59]			
	8		840±3[57]			
	20		845±3[57]		820±5,[46] 844±4(t.s.)	
	12		878±5[59]			
	40	837[50]	875±5[59]			
	132			813±9[58]		
	600		836[51]			
$NaAlSi_3O_8$	5		705±5[59]			
	8		704±5[57]			
	20		765±5[57]		678±3,[46] 683±5(t.s)	
	slow(?)	765[38]	763±11[58]			
	12	761[50]	737±5[59]			
	40		734±5[59]			
	132			763±11[58]		
	fast(?)			800±10[60]		
HPG8	300	864±5[39]	856[40]	856±3[40]	774±5(t.s.)	

[t.s.]: this study, in Ref. 54 T_g has been reported as corresponding to $10^{13·2}$ Pa s, in Ref. 60 T_g is for quenched sample
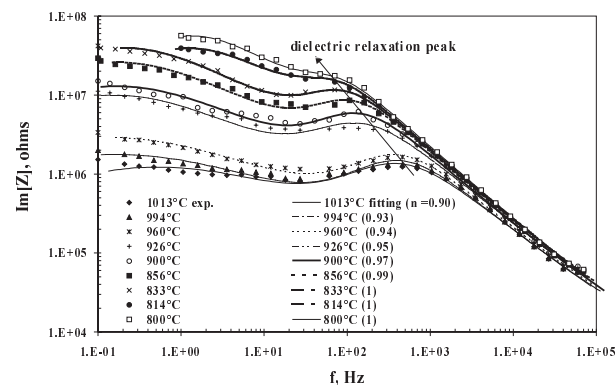
Figure 8. *Imaginary component of electrical impedance of anorthite at 0·3 GPa. The frequency scans of the electric impedance have been fitted to Equation (16) for each temperature. With the temperature increase the dielectric relaxation peak shifts toward high frequencies as indicated by the arrow. The deviation from Debye peak increases via decreasing parameter* n *(numbers in brackets). At* T>T$_g$ n *becomes less than 1. Anorthite glass is a fragile and 'tight' glassy conductor according to Ref. 36*

Figure 9. *Results of electrical resistance measurements in anorthite glass at 0·3 (upper panel) and 0·7 GPa (lower panel). The measurements of dc resistance at a fixed frequency are compared with bulk resistance obtained from Argand plots and fitting parameter R$_2$ in Equation (16). Bulk dc resistance measurements provide higher values of* T$_g$ *(solid arrows) in comparison with measurements at fixed frequency according to Ref. 35*

The fraction of nonbridging oxygens in albite and HPG8 structures is about zero. In silica glass, the electrical conductivity mechanism is a hopping process of OH$^-$ and alkali impurities between defect [AlO$_4$–M]^0 tetrahedra (AlO$_4$ alkalie metal centres), as well as the interconversion of charged NBO sites by hopping of polarons and electrons.[43,63] The relative effectiveness of a charge transport mechanism in glasses will depend on the average distance and the energetic barriers between neighbouring NBO sites or defected SiO$_4$ tetrahedra (hopping activation energy). It will depend also on the concentration of NBO sites and impurities and on the relative size of the hopping electric charge carriers (Na$^+$, K$^+$, Ca^{2+} or OH$^-$).

The highest electrical conductivity was observed in albite glass. In HPG8 glass Na ions are partially substituted by larger K ions, and the concentration of alkali ions is also smaller than in albite, Table 1. The least conductive of the feldspar glasses is anorthite. In anorthite glass the structure is less open compared to albite. Average interatomic distances are 1·63 and 1·66 Å for T–O, and 3·12 and 3·15 Å for T–T for albite and anorthite, respectively.[62] In anorthite Al and Si are the most ordered in comparison with other feldspar glasses, i.e. substitution of Al to Si is less random than in alkali aluminosilicates. Silica glass, Suprasil 300, used in this study possesses the lowest electrical conductivity due to much smaller concentration of defects, OH groups and [AlO$_4$–M]^0 tetrahedra. The lower values of σ_{dc} for SiO$_2$ and anorthite glasses in comparison with albite and haplogranitic glasses is due to the greater distances between NBO sites and other Si$^+$ and O$^-$ defects in the glass structure. Effectively, the longer distance for hopping electrical carriers results in fewer percolation paths for conduction.[63]

Experiments in piston cylinder

For high pressure experiments with a piston cylinder, samples of glasses were ground into powder and pressed into the gap between two coaxial electrodes, see Figure
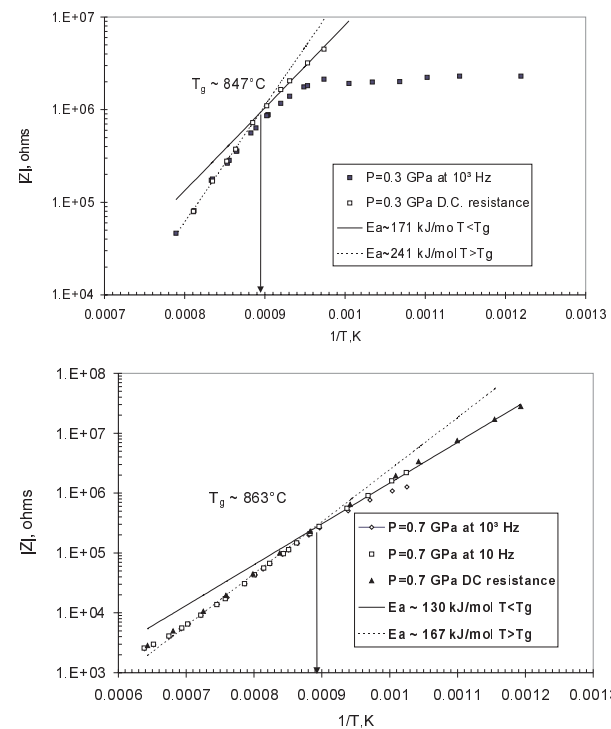
3. The bulk electrical conductivity was measured with a temperature step ca 10° and plotted on an Argand diagram. The electrical impedance data were collected in a scan with 0·17 log step of frequency from 10^{-1} to 10^5 Hz. Imaginary component of Z for anorthite glass in the glass transition temperature range is shown in Figure 8, which also demonstrates a low frequency peak due to electrode polarisation. The data for bulk resistance of anorthite presented on an Arrhenius plot demonstrate a significant change in the activation energy of $Z_{dc}=R_2$ of anorthite glass below and above T_g (see Figure 9) allowing the determination of T_g with an accuracy ±5°. In albite and HPG8 samples there is a noticeable frequency dependence of Z at low frequencies, Figure 10. Plotted in double log coordinates, the frequency dependence of Z allows estimation of a maximum frequency, F, at which the polarisation is observed at each temperature. The temperature dependence (Arrhenius plot) of the occurrence of this polarisation frequency F differs above and below T_g, providing an alternative way to estimate T_g, as it is shown in Figure 11. Both methods, Arrhenius plots of bulk resistance and polarisation frequency F, provide about the same result for T_g. The albite glass possesses a high electrical conductivity with a small activation energy, it may be classified as a 'loose' conductor. This class of conducting glasses has also a high polarisation (polarisation exponent $n\sim$0·5) and a broad dispersion range of dielectric properties.[35] The estimation of T_g in albite at 0·5 and 1 GPa are shown in Figure
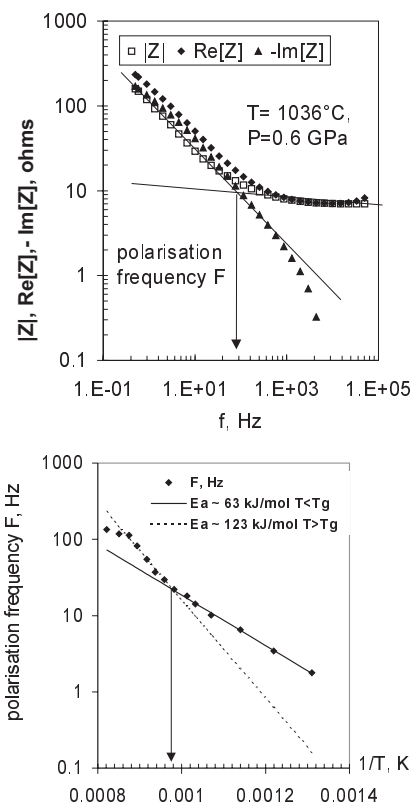
Figure 10. *Method of estimation of the polarisation frequency* F. *The intersection point of two derivatives dlog(Z')/dlog(f) calculated at* f≫1 Hz *and* f≪1 Hz, *corresponds to polarisation frequency* F *which was used for determination of 'mobile* Na-ion *T$_g$s' (left panel). At 0·6 GPa the data of polarisation frequency* F *(Hz) are plotted as a function of 1/*T,K. *Right panel is a polarisation frequency F, determined from frequency scans at different temperatures. The kink in the slope on the* F-*graph corresponds to the kink in the slope on the electrical impedance curve Figure 11*

12. For albite, as in the behaviour of viscosity versus pressure, T_g decreases with increasing pressure. The same effect of pressure is observed for the haplogranitic glass. For anorthite and silica glasses, T_g increases with pressure.

The data of electrical impedance *Im(Z)* for anorthite glass at 0·3 GPa and the results of fitting the frequency scan data to Equation (16) are shown in Figure 8. The temperature dependence of $\tau_{d.l.}$ determines the activation energy of the dielectric loss peak ~110 kJ/mol. The parameter *n* in Equation (16) characterises the broadness of the dielectric loss peak in comparison with a Debye peak (*n*=1). As follows from Figure 8, by crossing the glass transition temperature *n* becomes less than 1 (*n* ~0·95). Thus, the anorthite is fragile and 'tight' glassy conductor.[35] Silica glass is probably a strong and 'tight' glass having low electrical conductivity and polarisation exponent *n* is close to 1 and slightly decreases with the rising temperature, Figure 6. In the Argand diagram the bulk properties of SiO$_2$ glass are marked by a perfect semicircle, Figure 6. Estimation of T_g at 0·6 GPa in Suprasil 300 is shown in Figure 13. The difference in activation energies of σ_{dc} for SiO$_2$ and albite are very small, 142 and 148 kJ/mol, resulting in a significant error of T_g~1080±20°C, Figure 13.
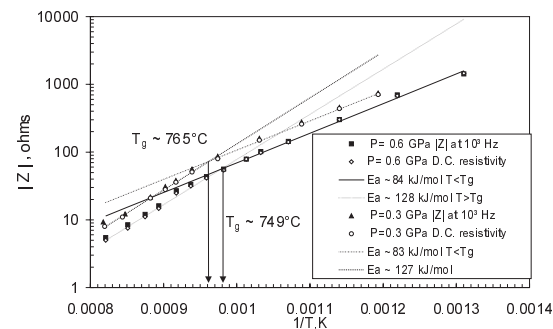
Figure 11. *Estimations of glass transition temperature from electric impedance measurements in HPG8 glass at 0·3 and 0·6 GPa at fixed frequency 10³ Hz and dc resistivity*

Experiments in belt apparatus and multi-anvil press

The results of electrical conductivity measurements carried out in the belt apparatus are shown in Figure 14. The change in the slope of the bulk conductivity below and above T_g is very small for anorthite as a result of increasing pressure and pressure dependent compressibility of the glass. In albite glass, the difference in the activation energy below and above T_g is significant. In reality, the kink of the slope in the dependence log(σ) versus 1/*T,K* for albite glass corresponds to 'mobile Na$^+$ T_gs' because of the presence of 'loose' species Na$^+$ in the structure.[35] Data[64] for albite glass at $T<T_g$ and pressures 3–4 GPa are in a good agreement with this study. With the pressure increase, the free volume becomes so small that above and below T_g the difference of activation energies of hopping
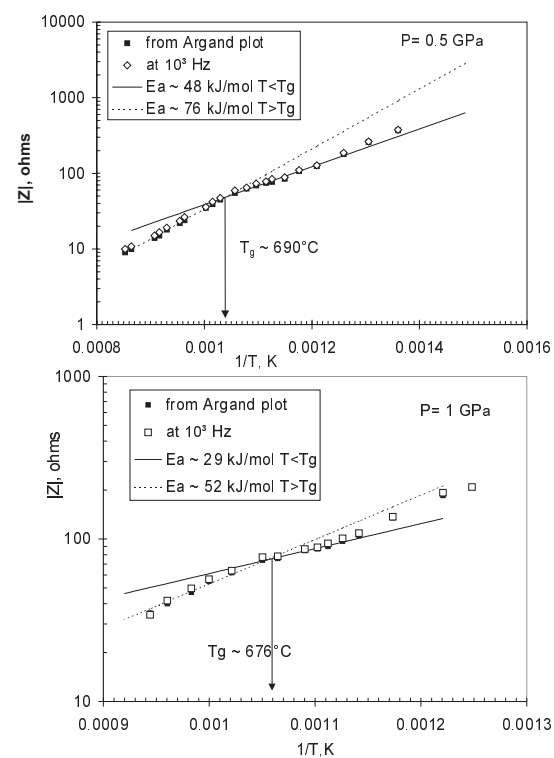

Figure 12. *Glass transition temperature in albite glass under pressure 0·5 (upper panel) and 1 GPa (lower panel). Arrows indicate* T$_g$, *the temperature point at which the activation energy starts to increase with the rising temperature*
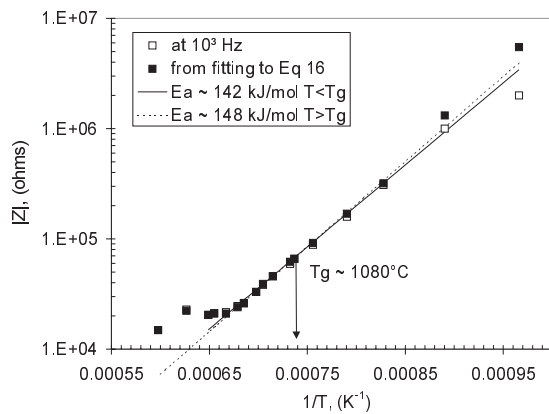
Figure 13. *Estimation of the glass transition temperature in SiO_2 Suprasil 300 at 0·6 GPa from the change in the activation energy of the dc resistance calculated from impedance frequency scans and Equation (16). The Argand plots are shown in Figure 6*

process of electrically charged defects or defect sites becomes negligible in the case of anorthite.[64,65] In albite glass, the activation energy of the bulk conductivity becomes smaller with the pressure increase. This may be explained by shortening of Na–Na distances in the albite structure, but the distance between Na site and the nearest oxygen remains the same. According to Ref. 34 the Coulomb barrier facing a mobile Na will be lowered by an increase of the electrostatic potential of a pair Na^+ and its empty site.

Only two experiments were done in the multi-anvil press on anorthite and albite glasses. T_g in both samples was very hard to detect, but likely corresponds to a maximum decrease of the bulk resistance on the
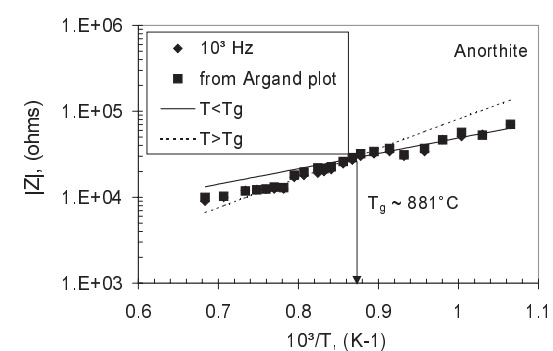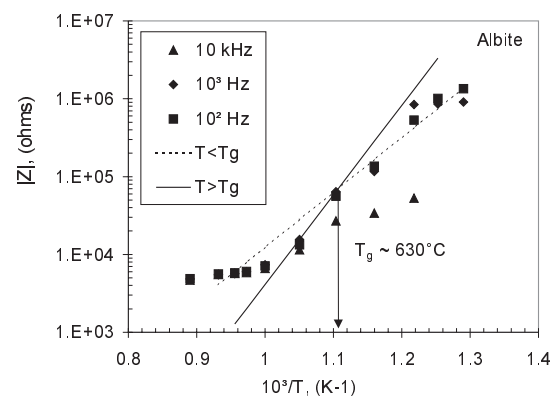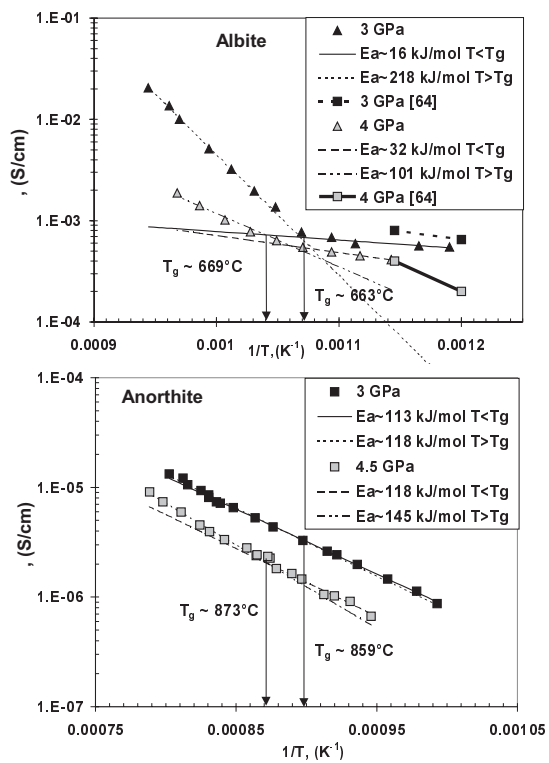

Figure 14. *Results of electrical conductivity and T_g measurements in the belt apparatus on albite (upper panel) and anorthite (lower panel) glass samples*

Figure 15. *Estimation of T_g at 6 GPa in multi-anvil press in albite (upper panel) and anorthite (lower panel). For albite the Argand plot was not possible to construct because of a low frequency noise, thus, only measurements at constant frequency (10^3 and 10^2 Hz) were used to identify T_g in the Arrhenius plot*

Arrhenius plot, Figure 15. The precision of T_g determination was about 15°C.

Discussion of results

Figure 16 represents a pressure dependence of the measured T_g from electrical impedance measurements in four type of experimental facilities: atmospheric furnace, piston cylinder, belt and multi anvil presses. For albite, and HPG8 the pressure dependence of T_g is negative, for SiO_2 and anorthite is positive. The high values of the T_g pressure derivative for HPG8 and SiO_2 are preliminary values, estimated for pressures below 0·6 GPa. Table 3 summarises the glass transition temperature estimated from electrical conductivity measurements in this study. The absolute value of the derivative dT_g/dP decreases
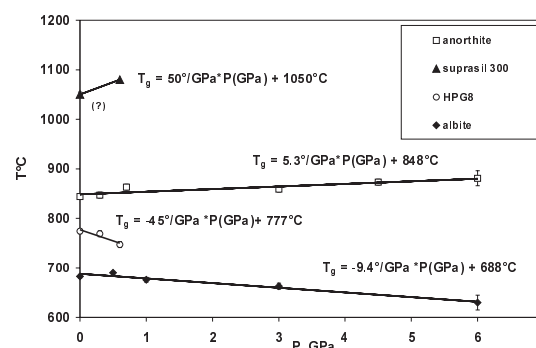

Figure 16. *Pressure dependence of the glass transition temperature from electrical impedance measurements. The slope of the pressure dependence of T_g at low pressures is higher than in the whole pressure range*

Table 3. *Results of* T_g *(°C) from electrical conductivity data (this study)*

Pressure (GPa)	Albite	Anorthite	HPG8	Suprasil 300
0·1 MPa	683±4	844±5	774±5	1050±10
0·3 GPa		847±6	769±6	
0·5	690±3			
0·6 (0·7*)		863±6*	747±6	1080±20
1	676±5			
3	663±5	859±6		
4·5		873±6		
6	630±15	881±15		

*measured at 0·7 GPa

with the pressure increase. However, as noted above, T_g is difficult to estimate at high pressures due to the pressure dependent compressibility. To detect a correct change in glass temperature with pressure at P=0·1 MPa perhaps only a short pressure interval is necessary (<0·1 GPa). Theoretically, the distribution of relaxation times will broaden at high pressure[66] and the transition occurs over a wider temperature range. This would make it impossible to detect T_g at some critical pressure. In the method which was used in this study, this happens when the activation energies of electrical conductivity below and above T_g become equal.

Table 4 lists previous estimations of the pressure dependence of T_g. Only one experimental investigation[67] reports results of *in situ* high pressure dilatometric measurements of T_g on glass samples having very fast cooling rates. dT_g/dP measured for diopside glass is in good agreement with calculated glass transition slope from the second Ehrenfest equation[47,68] and viscosity measurements.[6] The direct measurements of dT_g/dP on other glass formers indicate that the pressure dependence of T_g may vary from 200 to 150 K/GPa for B_2O_3 or lead[69] to 3·6 K/GPa for metallic glasses.[19]

The viscosity measurements in silicate melts provide explicit estimations of dT_g/dP. The rheology measurements of albite melt have been studied under pressure up to 7 GPa.[2,3] It was established that the decrease of albite melt viscosity is about 0·38 log[Pa s]/GPa. Using temperature dependence of viscosity of albite melt, the estimation of the pressure derivative of the glass transition temperature in albite is ~58 K/GPa.

The glass transition temperature in silica glass is the most poorly characterised because of the high resistivity of SiO_2 even at the highest experimental temperatures. T_g may vary from about 1200°C according to rheology data[70] and calorimetry[52] to 1100–1050°C according to high temperature light scattering experiments[18,56] depending on cooling rate, content of OH^-, and annealing temperature. The Prigogin–Defay ratio for SiO_2 glass Π ~2×10⁵ (!) is unexpectedly high, indicating that a single relaxation parameter cannot be used to describe a glassy state.[18]

In order to estimate a dielectric relaxation time from measured electrical impedance data (Z^*) the expressions for the complex modulus as follows were used[44]

$$M'-iM''=i\omega Z^*\varepsilon_0 G \tag{18}$$

where G is a geometric factor, ε_0 the dielectric constant of a free space and ω angular frequency.

Table 4. *Pressure dependence of glass transition temperature of some silicate glasses* dT_g/dP *(K/GPa)*

	Cooling rate	Diopside	Albite	Anorthite
1(67)	22–28 °C/min	+37±3	−25±10	
2(6)	calculated from viscosity	+34±14	−70±8	−4±17
3(68)		+49±3	+108±40	
Calculated from Eq 5 using ΔV^* and E_a of dielectric relaxation in this study	20°/h		−120±50	150±50
From electrical conductivity in this study	20°/h		−9·4±2	+5·3±1·5

[1] DTA measurements at pressures up to 0·7 GPa, [2] indirect estimations using WLF-equation at 0·1 MPa and the viscosity data at pressures up to 1·5 GPa (no cooling rate are reported), [3] calculated from thermodynamic data and Equation (6), no cooling rate reported. In the original paper this result is swapped with the result of Ref. 67

The dielectric relaxation times were calculated from frequency corresponding to a peak of M''

$$\tau=(2\pi f_{peak})^{-1} \tag{19}$$

The direct method to estimate a dielectric relaxation time is to make a fitting of the electrical impedance scans to an equivalent electric circuit, for example Equation (16), and estimate parameter $\tau_{d.1.}$. As a result of fitting of the second term in Equation (16), we get $\tau_{d.1.}$, the dielectric relaxation time, and n, polarisation exponent.[65] Both methods, Equations (16) and (19) must give the same result, if the impedance data only in the frequency band around dielectric relaxation peak are used. The activation energy of σ_{dc} may depend on temperature in the same way as $\tau=\sqrt{RC}$ where R is resistivity and C capacity at a peak frequency, only when R and C have the same activation energies and polarisation exponent n is close to 1.

The results of dielectric relaxation measurements for silicate glasses are presented in Figure 17, and the calculated activation energies of dielectric relaxation are listed in Table 4 and compared with the tracer diffusion activation energies. From Figure 17, the values of dielectric relaxation times of SiO_2 and anorthite are smaller than structural or shear stress relaxation for about 4–5 orders of magnitude, and for albite and haplogranite glass this difference is about 7–8 orders of magnitude. This difference in the decoupling index between structural and dielectric relaxation scales supports the idea that SiO_2 and anorthite are strongly coupled, albite and haplogranitic glasses are weakly couple glasses.[35] In strongly coupled glasses, SiO_2 and anorthite, this difference in activation energies is smaller than in albite, a weakly coupled glass.

The dielectric relaxation in weakly coupled glasses, alkaline silicates and alkaline aluminosilicates, has a substantial contribution from Na–Na site interactions lowering the energetic barrier of the hopping.[33] In the case of aluminosilicates, like albite and haplogranitic glass, the structural position of Na is near an oxygen belonging to AlO_4 complex.[34] In strongly coupled glasses, silica glass containing alkalis as impurities, the contribution into electric conductivity due to adjacent alkaline sites is negligible.

For SiO_2 the activation energy of dielectric relaxation below T_g is close to the tracer diffusion of Si ca.
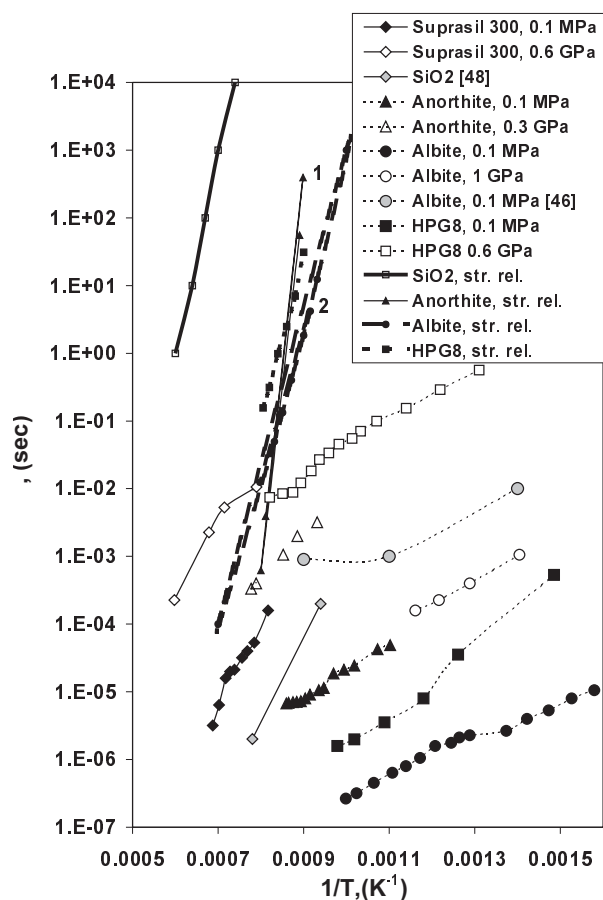
Figure 17. Temperature dependencies of dielectric versus structural relaxation time for silicate glasses. Dielectric relaxation time has been estimated from impedance measurements by using Equations (16) and (19). For HPG8 at 0·6 GPa the dielectric relaxation time is taken as 1/F, a reciprocal polarisation frequency. The structural relaxation time has been calculated from shear viscosity data at 0·1 MPa by using the Maxwell relationship τ(s)=η (Pas)/25 GPa. For SiO₂ (solid bold line) the data are from Ref. 48; for anorthite (solid thin line) the shear viscosity data are from Refs 58, 71, 72; for albite (dashed line): 1 shear viscosity from Refs 47, 71, 73; 2 from Refs 68, 74; for HPG8 (dotted line) the shear viscosity from Refs 7, 39, 75

220 kJ/mol. Above the glass transition, E_a of dielectric relaxation is close to E_a of O trace diffusion or structural relaxation ~515 kJ/mol.[48] According to the theoretical consideration in Ref. 34, the activation energy of the bulk conductivity/tracer diffusion in SiO₂ glass has to be equal to the binding energy of an isolated Na to oxygen in this glass ~130 kJ/mol. In this calculation, a distance Na–O is assumed 2·4 Å.[36] In that Na are at a dilute limit in SiO₂, the Coulomb barrier facing Na is not corrected for the attraction energy between a Na site and a nearest empty Na site. With the increase of Na content the activation energy of conductivity/tracer diffusion is equal to the binding energy Na–O corrected for (i.e. reduced by) the electrostatic energy of adjacent Na–Na sites and divided to the Kohlrausch exponent due to the cooperativity effects (or $(1-n)$, where n is the polarisation index Equation (16)). The distance between Na–Na in sodium silicates with a mole fraction of sodium ~0·3 is ~3·17 Å[36] and the correction factor for the cooperativity effects ~0·5. Thus, in fully polymerised

glasses, like albite or haplogranitic glass, the conductivity/tracer diffusion activation energy has to be ~60 kJ/mol, which was observed in this study at 0·1 MPa.

For anorthite, the reported activation energies are for chemical diffusion ~ 230–460 kJ/mol and significantly larger than measured E_a of dielectric relaxation 75–125 kJ/mol. The compiled data on tracer diffusion in the CaO–Al₂O₃–SiO₂ (40–20–40 wt%) system indicate that in the glass (600–900°C) E_a~245 (for ¹⁸O) and ~255 (for ³⁰Si) kJ/mol.[76] In the melt (1550–1350°C) E_a ~230 (for ²⁶Al), 290 (for ³¹Si) and ~380 (for ¹⁸O). In the supercooled liquid regime at temperatures just above T_g the activation energy for ¹⁸O tracer diffusion may even be 900 kJ/mol. Smaller activation energies for tracer diffusion of Ca, Al, Si and O were obtained from molecular dynamic simulations (MD), for anorthite glass (~110 kJ/mol), for melt (~180 kJ/mol).[77] The activation energy of dielectric relaxation in albite correlates well with the tracer diffusion of Na and differs from those of Si, Al and O. From MD simulations, the tracer diffusion coefficients in Ref. 78, have activation energies ~80 kJ/mol for Na, ~280 kJ/mol for Si, ~ 290 kJ/mol for O and ~270 kJ/mol for Al. In general, Ca²⁺ and Al³⁺ in silicate melts have rather low mobilities and their presence in the alkaline aluminosilicates may even impede the motion of alkali ions.[79]

The estimated T_g in albite glass from electrical impedance measurements characterises only a hopping and charge separation relaxation process of sodium and is not related to the structural relaxation. The same is probably true for HPG8. The small scale hopping and charge separation in the electric field is an effective mechanism of the electrical conductivity in sodium aluminosilicates.[80] The hopping of sodium ions between positions adjacent to *NBO* (in sodium silicates) and/or Al tetrahedra (in sodium aluminosilicates) sites may explain the high electrical conductivity of these glasses. The lower values of T_g estimated for albite and HPG8 from electrical impedance measurements in comparison with calorimetric and dilatometric data are indicators of the beginning of a 'loose' mobility of Na⁺ in the structure at temperatures even below rheological or calorimetric T_g, Table 2. The idea of a 'decoupling' character of dielectric relaxation from mechanical spectroscopy relaxation in sodium bearing glasses was discussed in detail in Ref. 81 on the basis of 'decoupling' index. Subsequently, the phenomena of alkaline tracer diffusion decoupling from structural relaxation was compiled and presented for geologists.[32,82] The activation energies of the dielectric relaxation time and of the diffusion coefficient are summarised in Table 5.

The pressure increase slows down the dielectric relaxation time. This may best be explained by a diminution of open paths and mobility of alkaline ions, increasing the time for defect diffusion. This correlates with the electrical conductivity measurements in Ag ionic glasses, where the pressure increase and densification results in a progressive decrease of the electrical conductivity.[31,28] The temperature dependence of dielectric relaxation in anorthite is plotted in

Table 5. *Activation energy of the diffusion coefficient and dielectric relaxation time (kJ/mol)*

Ions	SiO_2	$CalAl_2Si_2O_8$	$NaAlSi_3O_8$	$KAlSi_3O_8$ and HPG_8
OH⁻	83 (1100–500°C)[1]			
Si	237 (1200–800)[2]	230 (845–765)[6]	337 (1500–1100°C)[8]	
	579 (1410–1113)[3]			
O	48 (250°C)[4]	247 (760–760)[6]		
	516 (2500–1250°C)[5]			
Ca		327(1600–1350)[7]		
Al		462 (1600–1350)[7]	425 (1500–1100°C)[8]	
Na			56 (800–350)[9]	79 (800–350)[9]
K			99·5 (1000–350)[9]	63 (1000–350)[9]
E_a[10] in	222 (0·1 MPa, T<T_g)	74 (0·1 MPa)	43 (0·1 MPa, T<T_g)	98 (0·1 MPa, HPG8)
this	515 (0·1 MPa, T>T_g)	111 (0·3 GPa)	66 (0·1 MPa, T>T_g)	84 (0·3 GPa, HPG8)
study	~150 (0·6 GPa)	118 (4·5 GPa)	48 (0·5 GPa T<T_g)	40 (0·1MPa)[11]
			29 (1 GPa T<T_g)	
			16 (3 GPa *T<T_g*)	
			64 (0·1 MPa)[11]	

[1]effective OH diffusion,[83] [2]effective SiOSi diffusion,[83] [3]tracer diffusion ^{30}Si,[84] [4] ^{18}O diffusion in silica glass,[85] [5]estimated from viscosity measurements and Eyering equation,[86] [6]tracer diffusion of ^{18}O and ^{30}Si in CaAlSiO$_{4\cdot5}$,[84] [7]chemical diffusion of CaO/MgO and Al$_2$O$_3$ between diopside–anorthite compositions,[87] [8]self diffusion of Si and tracer diffusion Al/Ga,[88] [9]tracer diffusion of ^{24}Na and ^{42}K,[89] [10]E_a is the activation energy of dielectric relaxation (DR) measured in this study, [11]activation energy of dielectric relaxation calculated from electrical impedance data[46]

Figure 18 at three pressures 0·1 MPa, 0·3 and 4·5 GPa. The activation volume of τ for anorthite glass, calculated as follows

$$\Delta V^* = \frac{\partial \Delta E_a}{\partial P} \qquad (20)$$

is about +10·5 ± 5 cm³/mol. For albite glass, the pressure dependence of activation energy of conductivity at $T<T_g$ was used, Table 5, and the estimations provide a negative activation volume ~–6·5±2 cm³/mol. For comparison, MD simulations[78] of the tracer diffusion in albite provides for Na an activation volume ~3 cm³/mol, ~–4·5 cm³/mol for Al, ~–6 cm³/mol for Si and ~–5 cm³/mol for O. From the negative pressure dependence of viscosity the calculated activation volume of the shear viscosity in albite melt at 1900–2000 K and in pressure range 2·6–5·3 GPa is −5·4 cm³ mol⁻¹.[2] It should be noted here that the experimental error of the data in Figure 18 is rather large; the data were collected in three different apparatus (atmospheric pressure furnace, piston cylinder and belt apparatus), having differing sample geometries and temperature fields.

Table 6 summarises the literature data on parameters used in calculations of Prigogin–Defay parameter and the pressure dependence of T_g for studied silicate glasses. The span of parameter Π is one order
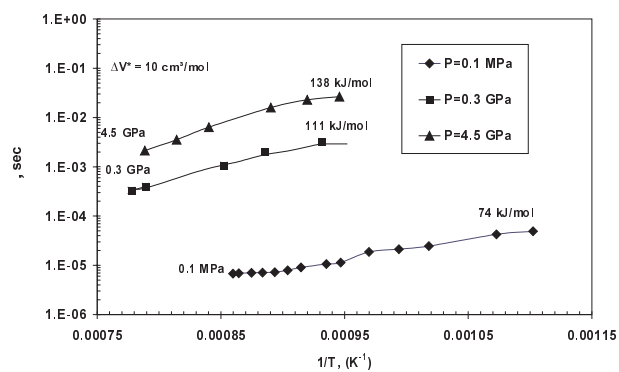
Figure 18. *Dielectric relaxation time of anorthite glass as a function of pressure. ΔV* is the activation volume calculated according to Equation (20) from the activation energy of the dielectric relaxation estimated at ~700–800°C*

of magnitude and, on average, it is much higher than 1 for all silicate glasses. The extreme high value of Π=1·7×10⁴ is calculated for SiO$_2$ by using the thermal expansion coefficient measurements from Ref. 53. However, if one uses the thermal expansivity data from Ref. 90, the value of Π for silica glass may be even close to 1. In the present work, the upper limit of Π estimated for SiO$_2$ glass by assuming that Δα~α from Ref. 53. In reality, the thermal expansion coefficient of silica glass is negative at temperatures up to 100–150°C above T_g and then above 2000 K, becomes again positive ~10⁻⁴ K⁻¹.[53] In Ref. 17 the α of SiO$_2$ was erroneously averaged in the wide temperature interval and the suggested Δα between silica glass and melt ~1·1×10⁻⁵ K⁻¹ is too small. For the calculation of Π for albite (from 15 to 3) and anorthite (from 38 to 7), the authors[17] used rather arbitrary values of Δβ (the contrast of isothermal compressibilities in glass and melt has been taken from 1 to 5×10⁻¹¹ Pa⁻¹). In the present estimation of Π, the experimental compressibility of melt was calculated by using the method of Ref. 95 and extrapolated data of Ref. 93. The contrast in compressibility between melt and glass was assumed to be 0·5β_T of the melt. In reality, Δβ_T may cover a much broader span. For example, in metallic glasses Δβ_T is about 1% of β_T,[19] in SiO$_2$ Δβ is about 75% of β.[18,96] For albite glass, the compressibility from the measurements of glass density at high pressure were also used.[94] A comparison between calculated and measured dT_g/dP in electrical impedance experiments indicates that only SiO$_2$ and anorthite (if only data at pressures <1 GPa are taken into account) are in a satisfactory agreement, Table 6. Otherwise, T_g and dT_g/dP estimated from electrical impedance data for alkaline aluminosilicates are very different from the structural glass transition. But even for anorthite, for which the present estimations of T_g are close to the structural glass transition, the Π value is much larger than 1, which does not permit consideration of the glass transition in anorthite as a second order phase transition, i.e. a relaxation process with one ordering parameter.

The results of T_g estimation from electrical impedance measurements provide different results in comparison with rheological, calorimetric or dilatometric

Table 6. *Prigogine–Defay ratio and pressure dependence of glass transition temperature*

Δ=liquid–glass	Anorthite	SiO$_2$	Albite	HPG8	Orthoclase
$\Delta\alpha\times10^{-5}$K^{-1}	2·3[58]	0·135[53]	0·76[58]	1·7[40]	0·8[58]
	1·9[50]	10·3[90]	3·3[91]		2·4[92]
	3·0[91]	1·1[17]			
$\Delta\beta\times10^{-11}$Pa^{-1}	2·5–2[93]	5·7[18]	4–3[94]	3·7³[93]	4·5–4³[93]
	1·9²[95]	6·3[96]	2·1²[95]	2·1²[95]	2·5²|
ΔC$_p$Jmol^{-1}K^{-1}	48[68]	8[68]	26·7[68]	8[98]	21·6[55]
	56·3[92]				37[92]
V$\times10^{-6}$m³mol^{-1}	110[58]	27·4[18]	112[58]	28·2[36]	112·1[97]
T$_g$K	1160[55]	1373[18]	1096[68]	1129[7,39]	1221[55]
	1109[51]	1460[68]	1036[92]	1073[98]	1178[92]
Π	22–1·5	7·6×10³–1·2	135–4·2	34–18	200–20
$(dT_g/dP)=(T_gV\Delta\alpha/\Delta C_p)$KGPa^{-1}	185–47	470–6	150–33	70–64	145–28
(dT_g/dP)KGPa^{-1}(ts)	5·3	50	–9·4	–45	
	30(P<1GPa)				

[1] calculated from Ref. 97; ² $\Delta\beta$ is a half of the calculated isothermal compressibility 0·5 β_T from Ref. 95; ³ data are extrapolated from Ref. 93; (ts) from electrical conductivity measurements, this study

measurements. There are few reasons for that. The question which arises, is it right to compare dynamic methods of T_g determination using variable frequency and methods using down and up scan definitions of T_g.[1] Usually, dynamic or ac methods result in higher values of T_g in comparison of time scanning of heating–cooling cycles. The observation in the present study of the small difference of T_g for anorthite and SiO$_2$ may be attributed to the difference in the definition of T_g: as the midpoint of the specific heat capacity rise in a heating temperature scan and as a temperature of the maximum in imaginary part of the electrical impedance. For alkaline bearing glasses the observed difference in T_g obtained from electrical measurements, on the one hand, and rheological, calorimetric or dilatometric studies, on the other, is more fundamental. Essentially, the difference in the relaxation time of mechanical and electric properties lies in the differing nature of contributions of these two relaxation and may attain a factor of 10^{12} near T_g for some glass formers.[30,35] In silicate glasses and melts containing Na$^+$ in the structure, the effects of charge separation are very important. Sodium is a highly unharmonic species, especially in the aluminosilicate structure. Sodium ions are responsible for a significant polarisation ($n\sim0\cdot5$ in Equation (16)). Ony replacing Si^{4+} by Al^{3+} sodium becomes surrounded by several nonbridging oxygen ions and aluminium tetrahedra. This results in an increase of the dielectric constant and increase of ionic polarasability with the increase of aluminium substitution.[80] The albite and haplogranitic glasses due to their high conductivity and polarasability can be classified as 'loose' glass formers. The T_g measured in these glasses by electrical impedance method is a temperature above which Na$^+$ ions become sufficiently mobile in comparison with the rest of the structure, and the kink in the slope $\ln(\sigma_{dc})$ versus $1/T,K$ corresponds to 'mobile Na ion T_g's'.[81] In other words, this break in the temperature of the secondary (Na ion mobility relaxation) at $T_g{}^{Na}$ is due to a persisting long range sodium mobility, while the long range motion of atoms constituting the rest of the structure (O, Si, Al) is almost frozen below $T_g{}^{Na}$.

The differing behaviour of the activation energy of the dielectric relaxation in anorthite and SiO$_2$, on the one hand, and albite and haplogranitic glass on the other, relates to the differing structures of these glasses. With the pressure increase, all interatomic distances in anorthite and SiO$_2$ become smaller due to the densification of their structures. Thus, the distances between alkaline cations and oxygen sites decreases, which result in an increase of the electrostatic binding energy and, therefore, the activation energy of electric conductivity. In alkaline bearing glasses like haplogranitic and albite glasses where alkali concentration is not at a dilute limit, sodium sites are mostly concentrated in channels and clusters due to a microsegregation of their structures.[34] Therefore, the pressure increase influences the distances between alkaline site in a larger extent than alkali–oxygen distances. As a result of this, under pressure the correction of the Coulomb binding energy will be lowered by an increasing electrostatic energy between alkali sites and the macroscopic activation energy of the electric conductivity decreases with pressure for these glasses.

Judging from the sign of dT_g/dP for studied glasses and qualitative behaviour of the fragility index *m* from Equations (10)–(12), it may be concluded that 'loose' conductive glasses (albite and haplogranite) become even more fragile with pressure increase, and 'tight' glasses (anorthite and SiO$_2$) are getting stronger under pressure. In other words, with the pressure increase and 'free volume' decrease, the charge carrier motions become increasingly oscillatory in alkali bearing glasses. This provides a further separation of slow diffusive from fast oscillatory modes.[35] In the case of albite or haplogranitic glass under pressure , the 'caging' effect of oxygen atom displacements may result in a highly decoupled diffusion motion for the 'loose' sodium atoms and in a reduction of 'the Na glass transition temperature' $T_g{}^{Na}$. This is associated with a decrease of the energetic barriers of sodium self diffusion and electric conductivity. In the case of anorthite and SiO$_2$ or insulating glasses, the 'caging' effect extends to all structural species reducing the gap between fast and slow modes. The energetic barriers for the diffusion motions

of atoms and the activation energy of electrical conductivity at T_g in these glasses increase under pressure.

Conclusions

1. The use of electrical impedance measurements to determine a glass transition temperature at high pressures provides results for anorthite and silica glasses consistent with previous studies. According to the structure of these glasses, the transport or diffusion of structural and electrically charged defects are correlated. Anorthite may be classified as a 'tight' fragile glass former, silica glass is a 'tight' strong glass. For albite and haplogranitic glasses the established T_g is not a structural glass transition because of the 'decoupling' between alkaline mobility/charge separation and structural relaxation, the estimated glass transition temperature is $T_g{}^{Na}$. These glasses belong to a class of 'loose' glassy conductors.

2. Pressure dependence of T_g estimated from electrical conductivity measurements reflects viscosity variations with pressure. For albite, the negative slope dT_g/dP corresponds to a decrease of the shear viscosity of albite melt under pressure. The greatest variation of T_g with pressure occurs at $P<1$ GPa. Further decrease of T_g is hindered by a decrease of percolation paths for conduction. As a result, the contrast between electrical conductivity below and above T_g becomes indistinguishable at pressures above 1 GPa.

3. Effect of pressure on dielectric relaxation times and the activation energy of dielectric relaxation may be explained in terms of the activation volume. A positive activation volume relates to a positive dT_g/dP and a 'tight' conductance behaviour under pressure (SiO_2, anorthite). A negative volume correlates with ae negative dT_g/dP (alkali bearing aluminosilicates at nondilute limit of alkali) and with a 'loose' electric conductance. This differing behaviour of dielectric relaxation under pressure correlates with the classification of glasses into two groups: glasses with strongly and with weakly coupled viscous and dielectric relaxations.

4. The dT_g/dP values determined when compared with those calculated from the second Ehrenfest relationship show a large discrepancy. Combined with the fact that a significant deviation of the Prigogin–Defay ratio from 1 is observed, this indicates a difference of the glass transition in silicates from the model of a second order phase transition. Qualitatively, the pressure dependence of T_g in silicate glasses correlates with a pressure dependence of the shear viscosity and thus the measurements of pressure dependence of T_g provide an indirect information of the melt rheology under pressure.

Acknowledgements

References

1. Angell, C. A. Glass transition. In *Encyclopaedia of materials: science and technology*. Volume 4. 2001. Edited by Buschow *et al* Elsevier, Amsterdam. Pp 3565–75.
2. Suzuki, A., Ohtani, E., Funakoshi, F. & Terasaki, H. Viscosity of albite melt at high pressure and high temperature. *Phys. Chem. Miner.*, 2002, **29**, 159–65.
3. Kushiro, I. Viscosity and structural changes of albite ($NaAlSi_3O_8$) melt at high pressures. *Earth Planet. Sci. Lett.*, 1978, **41**, 87–90.
4. Shaw, H. R. Viscosities of magmatic silicate liquids: an empirical method of prediction. *Am. J. Sci.*, 1972, **272**, 870–93.
5. Persikov, E. S., Zharikov, V. A., Bukhtiyarov, P. G. & Pol'skoy, S. F. The effect of volatiles on the properties of magmatic melts. *Eur. J. Miner.*, 1990, **2**, 621–42.
6. Taniguchi, H. Universal viscosity-equation for silicate melts over wide temperature and pressure ranges. *J. Vocanol. Geotherm. Res.*, 1995, **66**, 1–8.
7. Hess, K-U., Dingwell, D. B. & Webb, S. L. The influence of excess of alkalis on the viscosity of a haplogranitic melt. *Am. Miner.*, 1995, **80**, 297–304.
8. Hess, K-U. & Dingwell, D. B. Viscosities of hydrous leucogranitic melts: a non-Arrhenian model. *Am. Miner.*, 1996, **81**, 1297–300.
9. Cooper, A. R. & Gupta, P. K. A dimensionless parameter to characterise the glass transition. *Phys. Chem. Glasses*, 1982, **23** (1), 44–5.
10. Mazurin, O. V. *Vitrification*. 1986. Nauka, Leningrad, Pp 158. (In Russian.)
11. Gutzow, I., Dobreva, A., Rüssel, C. & Durschang, B. Kinetics of vitrification under hydrostatic pressure and under tangential stress. *J. Non-Cryst. Solids*, 1997, **215**, 313–19.
12. Bianchi, U. Pressure effects on glass transition in polymers. *J. Phys. Chem.*, 1965, **69** (5), 1497–1504.
13. Goldstein, M. Viscous liquids and the glass transition. IV. Thermodynamic equations and the transition. *J. Phys. Chem.*, 1973, **77** (5), 667–73.
14. Nieuwenhuizen, T. M. Ehrenfest relations at the glass transition: solution to an old paradox. *Phys. Rev. Lett.*, 1997, **79** (7), 1317–20.
15. Speedy, R. J. Revised Ehrenfest relations for the glass transition. *J. Phys. Chem. B*, 1999, **103**, 8128–31.
16. Bianchi, U., Turturro, A. & Basile, G. Pressure effect on glass transition in polymers. II. A study of the factors affecting dT_g/dP values. *J. Phys. Chem.*, 1967, **71**(11), 3555–8.
17. Dingwell, D. B., Knoche, R. & Webb, S. A volume temperature relationship for liquid GeO_2 and some geophysically relevant derived parameters for network liquids. *Phys. Chem. Miner.*, 1993, **19**, 445–53.
18. Krol, D. M., Lyons, K. B., Brawer, S. A. & Kurkjian, C. R. High temperature light scattering and the glass transition in vitreous silica. *Phys. Rev. B*, 1986, **33**, 4196–202.
19. Samwer, K., Busch, R. & Johnson, W. L. Change of compressibility at the glass transition and Prigogine-Defay ratio in ZrTiCuNiBe alloys. *Phys Rev. Lett.*, 1999, **82** (3), 580–3.
20. Jäckle, J. Models of glass transition. *Rep. Prog. Phys.*, 1986, **49**, 171–231.
21. Skorodumov, V. F. Thermodynamic aspects of glass-formation under pressure. *Zh. Fiz. Khim.*, 1994, **69** (12), 2254–6. (In Russian.)
22. Paluch, M., Rzoska, S. J. & Zioło, J. On the isothermal pressure behaviour of the relaxation times for supercooled glass-forming liquids. *J. Phys. Condens. Matter*, 1998, **10**, 4131–8.
23. Munro, R.G., Block, S. & Piermarini, G. J. Correlation of the glass transition and the pressure dependence of viscosity in liquids. *J. Appl. Phys.*, 1979, **50** (11), 6779–83.
24. Oliver, W. F., Herbst, C. A. & Wolf, G. H. Viscous liquids and glasses under high pressure. *J. Non-Cryst. Solids*, 1991, **131–133**, 84–7.
25. Leyser, H., Schulte, A., Doster, W. & Petry, W. High-pressure specific-heat spectroscopy at the glass transition in o-terphenyl. *Phys. Rev. E*, 1995, **51** (6), 5899–904.
26. Paluch, M., Zioło, J. & Rzoska, S. *Phys. Rev. E*, 1997, **56** (5), 5764–7.
27. Böhmer, R., Ngai , K. L., Angell, C. A. & Plazek, D. J. Nonexponential relaxation in strong and fragile glass formers. *J. Chem. Phys.*, 1993, **99** (5), 4201–9.
28. Avramov, I. Viscosity of glass forming melts. *J. Non-Cryst. Solids*, 1998, **238**, 6–10.
29. Avramov, I. Pressure dependence of viscosity of glass forming melts. *J. Non-Cryst. Solids*, 2000, **262**, 258–63.
30. Angell, C. A. Phenomenology of fast ion conducting glasses: facts and confusion. In *High temperature superionic conductors*. 1989. Edited by T. Takahashi. World Scientific, Singapore. Pp 89–113.
31. Hutchinson, J. M., Ingram, M. D. & Robertson, A. H. J. The effect of pressure and densification on ionic conductivities in silver

iodomolybdate glasses. *Phil. Mag. B*, 1992, **66**, 449–61.
32. Dingwell, D. Effects of structural relaxation on cationic tracer diffusion in silicate melts. *Chem. Geol.*, 1990, **82**, 209–16.
33. Kahnt, H. Ionic transport in glasses. *J. Non-Cryst. Solids*, 1996, **203**, 225–31.
34. Greaves, G. N. & Ngai, K. L. Reconciling ionic-transport properties with atomic structure in oxide glasses. *Phys. Rev. B*, 1995, **52**, 6358–80.
35. Angell, C. A. The nature of glassforming liquids, the origin of superionics and 'tight' vs. 'loose' glassy conductors *Solid State Ionics,* 1998, **105**, 15–24.
36. Huang, C. & Cormack, A. N. The structure of sodium silicate glass. *J. Phys. Chem.*, 1990, **93**, 8180–6.
37. Sidebottom, D. L. Dimensionality dependence of the conductivity dispersion in ionic materials. *Phys. Rev. Lett.*, 1990, **83**, 983–6.
38. Angell, C. A., Moynihan, C. T. & Hemmati, M. 'Strong' and 'superstrong' liquids, and an approach to the perfect glass state via phase transition. *J. Non-Cryst. Solids*, 2000, **275**, 319–31.
39. Hess, K-U. Zur Temperaturabhängigkeit der Viskosität von haplogranitischen Schmelzen. *Dissertation zur Erlangung des Grades Doktor der Naturwissenschaften.* 1996. Universität Bayreuth. Pp 115.
40. Knoche, R., Dingwell, D. B. & Webb, S. L. Melt densities for leucogranites and granitic pegmatites: Partial molar volumes for SiO$_2$, Al$_2$O$_3$, Na$_2$O, K$_2$O, Li$_2$O, Rb$_2$O, Cs$_2$O, MgO, CaO, SrO, BaO, B$_2$O$_3$, P$_2$O$_5$, F$_2$O$_{-1}$, TiO$_2$, Nb$_2$O$_5$, Ta$_2$O$_5$ and WO$_3$. *Geochim. Cosmochim. Acta*, 1995, **59**, 4645–52.
41. Bagdassarov, N., Freiheit, H. & Putnis, A. Ionic conductivity and pressure dependence of trigonal-to-cubic phase transition in lithium sodium sulphate. *Solid State Ionics*, 2001, **143**, 285–96.
42. Brey, G. P., Weber, R. & Nickel, K. G. Calibration of a belt apparatus up to 1800°C and 6 GPa *J. Geophys. Res. B*, 1990, **95** (10), 15,603–10.
43. Xu ,Y., Poe, B. T., Shankland, T. J. & Rubie, D. C. Electrical conductivity of olivine, wadsleyite, and ringwoodite under upper-mantle conditions. *Science*, 1998, **280**, 1415–18.
44. MacDonald, J. R. *Impedance spectroscopy: emphasising solid materials and systems.* 1987. Wiley, New York. P 7.
45. Fritzsche, T. Impedanzmessungen an Gläsern des Systems Albit-Nephelin im Glastransformations-Bereich. *Dissertation zur Erlangung des Doktorgrades der Mathematisch-Naturwissenschaflichen Fachberreiche der Georg-August-Univers*ität, Göttingen. 1990. Pp 122.
46. Fuchser, D. Impedanzspektroskopische und kalorimetrische Untersuchungen an silikstischen Gläsern. *Dissertation zur Erlangung des Doktorsgrades der Mathematisch-Naturwissenschaflichen Fachberreiche der Georg-August-Universität*, Göttingen. 1996. Pp 127.
47. Hayward, R. J. The mixed alkali effect in aluminosilicate glasses. Part 1. The join SiO$_2$-(Na,K)AlSi$_3$O$_8$. *Phys. Chem. Glasses*, 1976, **17** (3), 54–61.
48. Kakuichida, H., Saito, K. & Ikushima, A. J. Dielectric relaxation in silica glass. *J. Appl. Phys.*, 1999, **86**, 5983–7.
49. Del Frate, D., Quilici, S., Spinolo, G. & Vedda, A. High-temperature ac conductivity of amorphous SiO$_2$: fused silica and thin thermal films. *Phys. Rev. B*, 1999, **59**, 9741–4.
50. Richet, P. Viscosity and configurational entropy of silicate melts. *Geochim. Cosmochim. Acta*, 1984, **48**, 471–83.
51. Moynihan, C. T. Structural relaxation and the glass transition. In *Structure, dynamics and properties of silicate melts.* Volume 32. 1995. Edited by J. F. Stebbins, P. F. McMillan & D. B. Dingwell. Reviews in Mineralogy, MSA. Pp 1–20.
52. Richer, P., Bottinga, Y., Denilou, L., Petitet, J.&Tequi, C. Thermodynamic properties of quartz, crystoballite and amorphous SiO$_2$: drop calorimetry measurements between 1000 and 1800K and a review from 0 to 2000K. *Geochim. Cosmochim. Acta*, 1982, **46**, 2639–58.
53. Brückner, R. Properties and structure of vitreous silica. I. *J. Non-Cryst. Solids*, 1970, **5**, 123–75.
54. Brückner, R. Charakteristische physikalische Eigenschaften der oxidischen Hauptglasbildner und ihre Beziehung zur Struktur der Gläser. Teil I. Schmelz und Viskositätsverhalten der Hauptglasbildner. *Glastech. Ber.,* 1964, **37**, 413–25.
55. Richet, P. & Bottinga, Y. Glass transition and thermodynamic properties of amorphous SiO$_2$, NaAlSi$_n$O$_{n+2}$ and KAlSi$_3$O$_8$. *Geochim. Cosmochim. Acta*, 1984, **48**, 453–70.
56. Saito, K., Kakiuchida H. & Ikushima, A. J. Light-scattering study of the glass transition in silica with practical implications. *J. Appl. Phys.*, 1998, **84**, 3107–12.
57. Martens, R. M. Kalorimetrische Untersuchungen der kinetischen Parameter im Glastransformationsbereich bei Gläsern im System Diopsid-Anorthit-Albit und bei einem NBS-710-Standardglas. *Frankfurter Geowissenschaftliche Arbeiten, Serie C – Mineralogie*. 1985. Universität Frankfurt. Pp 180.
58. Arndt, J. & Häberle, F. Thermal expansion and glass transition temperatures of synthetic glasses of plagioclase-like compositions. *Contrib. Miner. Petrol.*, 1973, **39**, 175–83.
59. Knoche, R., Dingwell, D. B. & Webb, S. L. Non-linear temperature dependence of liquid volumes in the system albite-anorthite-dopside. *Contrib. Mineral. Petrol.,* 1992, **111**, 61–73; Knoche, R. Untersuchungen der Glastransformationstemperatur im Sytem

Albit-Anothit-Diopsid mit Hilfe der DTA. *Diplomarbeit, Mineralogisch-Petrologische Institut.* 1990. Universität zu Göttingen, Göttingen. Pp 92.
60. Ochs, F. A., III & Lange, R. A. The partial volume, thermal expansivity, and compressibility of H2O on NaAlSi$_3$O$_8$ liquid: new measurements and an internally consisted model. *Contrib. Miner. Petrol.*, 1997, **129**, 155–65.
61. Meaudre, M. & Meaudre, R. AC conduction in r.f. sputtered SiO$_2$ films. *Phil. Mag. B*, 1979, **40**, 401–10.
62. Taylor, M. & Brown, G. E. Structure on mineral glasses . I. The feldspar glasses NaAlSi$_3$O$_8$, KAlSi$_3$O$_8$, CaAl$_2$Si$_2$O$_8$. *Geochim. Cosmochim. Acta*, 1979, **43**, 61–75.
63. Meaudre, R. & Meaudre, M. Bipolar and single-polaron contributions to ac conduction in r.f. sputtered SiO$_2$ films. *Phil. Mag.*, 1982, **46**, 647–57.
64. Vornehm, M. Elektrische Leitfähigkeit von Plagioklasgläsern in Abhängigkeit von Druck und Temperatur. *Dissertation zur Erlangung der Doktorsgrades.* 1976. Universität zu Tübingen, Tübingen. Pp 97.
65. Jonscher, A. K. Dielectric relaxation in solids. *J. Phys. D*, 1999, **32**, R57–70.
66. O'Reilly J.M. Effect of pressure on amorphous polymers. In *Modern aspects of vitreous state*. Volume 3. 1960. Edited by J. D. MacKenzie. Butterworths, London. Pp 59–89.
67. Rosenhauer, M., Scarfe, C.M. & Virgo, D. Pressure dependence of the glass transition temperature in glasses of diopside, albite, and sodium trisilicate composition. In *Carnegie Institute Yearbook 1978-79*. 1979. Carnegie Geophysical Laboratory, Washington D C. Pp 557–9.
68. Richet, P. & Bottinga, Y. Anorthite, andesite, wollastonite, diopside, cordierite and pyrope: thermodynamics of melting, glass transitions, and properties of the amorphous phases. *Earth Planet. Sci. Lett.*, 1984, **67**, 415–32.
69. Angell, C. A., Pollard, L.J . & Strauss, W. Effect of pressure on the electrical conductance and glass-transition temperature of molten nitrates. *J. Chem. Phys.,* 1965, **43** (8), 2899–900.
70. Richert, R. & Angell, C. A. Dynamic of glass-forming liquids. V. On the link between molecular dynamics and configurational entropy. *J. Chem. Phys.,* 1998, **108**, 9016–26.
71. Tauber, P. Viskositätsuntersuchungen im Modellsystem Anorthit-Albit-Diopsid. *Dissertation zur Erlangung der Doktorgrades.* 1987. Universität zu Tübingen, Tübingen. Pp 79.
72. Tauber, P. & Arndt, J. The relationship between viscosity and temperature in the system anorthite-diopside. *Chem. Geology*, 1987, **62**, 71–81.
73. Tauber, P. & Arndt, J. Viscosity–temperature relationship in liquid diopside. *Phys. Earth Planet. Int.,* 1986, **43**, 97–103.
74. Knoche, R., Dingwell, D. B. & Webb, S. L. Non-linear temperature dependence of liquid volumes in the system albite-anorthite-diopside. *Contrib. Miner. Petrol.,* 1993, **111**, 61–73.
75. Dorfman, A. M., Hess, K-U. & Dingwell, D. B. Centrifuge assisted falling sphere viscometry. *Eur. J. Miner.,* 1996, **8**, 507–14.
76. Chakraborty, S. Diffusion in silicate melts. In *Structure, dynamics and properties of silicate melts*. Volume 32. 1995. Edited by J. F. Stebbins, P. F. McMillan & D. B. Dingwell . Reviews in Mineralogy, MSA. Pp 411–504.
77. Morgan, N. A. & Spera, F. J. Glass transition, structural relaxation and theories of viscosity: a dynamics study of amorphous CaAl$_2$Si$_2$O$_8$. *Geochim Cosmochim Acta*, 2001, **65** (21), 4019–404.
78. Bryce, J. G., Spera, F. J. & Stein, D. J. Pressure dependence of self-diffusion in the NaAlO$_2$–SiO$_2$ system. Compositional effect and mechanisms. *Am. Miner.,* 1999, **84**, 345–56.
79. MacKenzie, J. D. Semiconducting oxide glasses. In *Modern aspects of the vitreous state*. Volume 2. 1960. Edited by J. D. MacKenzie. Butterworths, London. Pp 126–48.
80. Hsieh, C. H., Jain, H. & Kamitsos, E. I. Correlation between dielectric constant and chemical structure of sodium silicate glasses. *J. Appl. Phys.,* 1996, **80** (3), 1704–12.
81. Angell, C. A. Structural instability and relaxationin liquids and glassy phases near the fragile liquid limit. *J. Non-Cryst. Solids*, 1988, **102**, 205–21.
82. Dingwell, D. B. & Webb, S. L. Relaxation in silicate melts. *Eur. J. Miner.*, 1990, **2**, 427–49.
83. Davis, K. M. & Tomozawa, M. Water diffusion into silica glass: structural changes in silica glass and their effect on water solubility and diffusivity. *J. Non-Cryst. Solids,* 1995, **185**, 203–20.
84. Freer, R. Diffusion in silicate minerals and glasses: a data digest and guide to the literature. *Contr. Miner. Petrol.,* 1981, **76**, 440–54.
85. García-Rodriguez, F. J., Pérez-Robles, F., Manzano-Ramírez, A., Vorobiev, Y. V. & Gozález-Hernández, J. Oxygen diffusion in silica glass prepared by sol-gel method. *Solid State Commun.,* 1999, **111**, 717–21.
86. Henmmati, M. & Angell, C. A. Comparison of pair-potential models for the simulation of liquid SiO$_2$: Thermodynamics, angular-distribution and diffusional properties. In *Physics meets mineralogy*. 2000. Edited by H. Aoki, Y. Syono & R. J. Hemley. Cambridge University Press, Cambridge. Pp 325–39.
87. Kubicki, J. D., Muncill, G. E. & Lasaga, A. C. Chemical diffusion in

melts on the $CaMgSi_2O_6$–$CaAl_2Si_2O_8$ join under high pressures. *Geochim. Cosmochim. Acta,* 1990, **54**, 2709–15.

88. Baker, D. R. Diffusion of silicon and gallium (as an analogue for aluminium) network-forming cations and their relationship to viscosity in albite melt. *Geochim. Cosmochim. Acta,* 1995, **59**, 3561–71.

89. Jambon, A. & Carron, J-P. Diffusion of Na, K, Rb and Cs in glasses of albite and orthoclase composition. *Geochim. Cosmochim. Acta,* 1976, **40**, 897–903.

90. Bacon, J. F., Hasapis, A. A. & Wholley, J. W. Viscosity and density of molten silica and high silica content glasses. *Phys Chem Glasses,* 1960, **1** (3), 90–8.

91. Knoche R. Temperaturabhängige Eigenschaften silikatischer Schmelzen. *Dissertation zur Erlangung des Doktorsgrades der Fakultät Geowissenschaften.* 1993. Universität Bayreuth., Bayreuth. Pp 186.

92. Carmichael, I. S. E. Glass and the glassy rocks. In *The evolution of the igneous rocks.* Princeton University Press, Princeton. 1979. Pp 233–44.

93. Rivers, M. L. & Carmichael, I. S. E. Ultrasonic studies of silicate melts. *J. Geophys. Res.,* 1987, **92**, 9247–70.

94. Navrotky, A., Fukuyama, H. & Davies P. K. Calorimetric studies of crystalline and glassy high pressure phases. In *Annual reviews of earth and planetary sciences.* Volume 12. 1982. Edited by S. Akimoto & M. H. Manghnani. Pp 465–77.

95. Kress, V. & Carmichael, I. S. E. The compressibility of silicate liquids containing Fe_2O_3 and the effect of composition, temperature, oxygen fugacity and pressure on their redox states. *Contrib. Miner. Petrol.*, 1991, **108**, 82–92.

96. Bucaro, J. A. & Dardy, H. D. High-temperature Brillouin scattering in fused quartz. *J. Appl. Phys.,* 1974, **45**, 5324–9.

97. Bottinga, Y., Weill, D. & Richet, P. Density calculations for silicate liquids. 1. Revised method for aluminosilicate compositions. *Geochim. Cosmochim. Acta,* 1982, **46**, 909–19.

98. Toplis, M. J., Gottsmann, J., Knoche, R. & Dingwell, D. Heat capacities of haplogranitic glasses and liquids. *Geochim. Cosmochim. Acta*, 2001, **65**(14), 1985–94.